PERPENDICULAR FIBER TRACKING FOR FIBER BUNDLE ANALYSIS

By

SIDDHARTH RAY

A THESIS PRESENTED TO THE GRADUATE SCHOOL
OF THE UNIVERSITY OF FLORIDA IN PARTIAL FULFILLMENT
OF THE REQUIREMENTS FOR THE DEGREE OF
MASTER OF SCIENCE

UNIVERSITY OF FLORIDA

2012

© 2012 Siddharth Ray

Dedicated to my parents

ACKNOWLEDGMENTS

I would first and foremost like to express my deep gratitude to my advisor Dr. Walter G. O'Dell for his guidance during my research. He was available every time I needed clarifications and numerous discussions with him guided me through the project. His support and guidance throughout these years in graduate school have made it a very productive and enjoyable experience.

My sincere thanks extend to Dr. Angelos Barmpoutis, who was like my second advisor, for the generous support and encouragement to submit my work in various conferences. I would also like to thank Dr. Paul R. Carney, my committee member, for the comments enabling me to understand the caveats of that rat experiments and Dr. Mansi Parekh for providing me real DW-MRI rat brain datasets.

I would like to extend my gratitude towards my fellow lab mates Ankit Salgia, Rujuta Munje and Jiucheng Nie for numerous useful discussions and all the fun time we had. I would also thank Tifiny D. McDonald for administrative and friendly support during various occasions.

Finally, I sincerely thank my parents, brother and my girlfriend for being supportive and understanding during stressful and happy times.

I acknowledge funding support from Shands Cancer Center, University of Florida.

TABLE OF CONTENTS

page

ACKNOWLEDGMENTS 4

LIST OF TABLES 7

LIST OF FIGURES 8

ABSTRACT 10

CHAPTER

1 INTRODUCTION 12

1.1 Objectives 12
1.2 Clinical Motivation 12
1.3 Current Methods for Diagnosing and Treating Brain Diseases/Disorders 13
1.4 Need for Improvement 14
1.5 Organization of Report 15

2 METHODS 16

2.1 Background 16
2.2 Magnetic Resonance Diffusion Tensor Imaging (MR-DTI) 16
2.3 Fiber Tracking 18
2.3.1 Deterministic Tractography 19
2.3.2 Probabilistic Tractography 21
2.3.3 Combination of Deterministic and Probabilistic Tractography 22
2.4 Method 22
2.4.1 DTI Reconstruction 22
2.4.4 Perpendicular Fiber Tracking 24
2.4.4.1 Geometric cost 25
2.4.4.2 Fiber cost 26
2.4.4.3 Total cost function 27
2.4.4.4 Thresholds 27
2.4.5 Construction of 3D Cost Maps Through Dynamic Programming 28
2.4.6 Algorithm: Pseudocode for 3D DP for Perpendicular Fiber Tracking 30

3 TOWARDS VERIFICATION OF PERPENDICULAR FIBER TRACKING 31

3.1 Validation on Synthetic Datasets 31
3.2 Generation of Synthetic Dataset 31
3.3 Implementation 31
3.4 Specifications 32
3.5 Data Set 1: Inclined Fibers 32
3.6 Data Set 2: Conical Bundle with Parallel Fibers 34

3.7 Data Set 3: Linear and Curving Fibers 36
3.8 Data Set 4: Fibers Branching 39

4 RESULTS 41

4.1 Application on Real Datasets 41
4.2 Implementation 41
4.3 Pre-processing 41
4.4 Rat Hippocampus 43
4.4.1 Data Acquisition 43
4.4.2 Fiber Bundle Analysis Using Perpendicular Fiber Tracking 44
4.4.3 Discussions 47
4.5 Control and Disease (Epilepsy) Rat Brain 50
4.5.1 Data Acquisition 51
4.5.2 Fiber Bundle Analysis of Control and Disease Rat Brain 51
4.5.3 Discussion 64

5 CONCLUSIONS AND FUTURE WORK 65

5.1 Conclusions 65
5.2 Limitations 65
5.3 Future Work 66
5.3.1 Improvement of Perpendicular Fiber Tracking Method 66
5.3.2 Application on Real Datasets 66

LIST OF REFERENCES 68

BIOGRAPHICAL SKETCH 70

LIST OF TABLES

Table page

2-1 List the factors and their formulation..... 25

LIST OF FIGURES

Figure page

2-1 Diffusion encoding gradients 17

2-2 Illustration of fiber trajectory 19

2-3 Illustration of streamline and Fiber Assignment by Continuous Tracking (FACT) method of tractography.. 20

2-4 Connectivity distribution with seed point in posterior limb..... 21

2-5 Illustration of Split and Merge Tractography (SMT) 22

2-6 Illustration of steps perpendicular fiber tracking..... 24

2-7 Geometric cost 26

2-8 Fiber cost..... 26

2-9 Dynamic Programming 29

3-1 Results from synthetic dataset#1..... 34

3-2 Results from synthetic dataset#2..... 35

3-3 Ellipsoidal representation of eigenvectors for dataset#3. 36

3-4 Results from synthetic dataset#3..... 37

3-5 Results from synthetic dataset#3..... 38

3-6 Ellipsoidal representation for eigenvectors of fibers branching..... 39

3-7 Results from synthetic dataset#4..... 40

4-1 Surf plots of a rat brain DWI dataset..... 42

4-2 Shown is the FA map 43

4-3 Results obtained from analysis of the rat hippocampus with seed point in the stratum lacunosum-moleculare..... 46

4-4 Results obtained from analysis of the rat hippocampus with seed point in the stratum oriens..... 47

4-5 Visual depiction of the extend of the reconstructed fiber bundle in the stratum lacunosum-moleculare 48

4-6 Visual depiction of the extend of the reconstructed fiber bundle in the Stratum oriens 48

4-7 [A] Shown is the colored FA map of control rat brain dataset 50

4-8 Results obtained from analysis of the rat brain with seed point shown with black marker 52

4-9 Results obtained from analysis of the rat brain with seed point shown with black marker 53

4-10 Results obtained from analysis of the rat brain with seed point shown with black marker 54

4-11 Results obtained from analysis of the rat brain with seed point shown with black marker 55

4-12 Results obtained from analysis of the rat brain with seed point shown with black marker 56

4-13 Results obtained from analysis of the rat brain with seed point shown with black marker 57

4-14 Results obtained from analysis of the rat brain with seed point shown with black marker 58

4-15 Results obtained from analysis of the rat brain with seed point shown with black marker 59

4-16 Results obtained from analysis of the rat brain with seed point shown with black marker 60

4-17 Results obtained from analysis of the rat brain with seed point shown with black marker 61

4-18 Results obtained from analysis of the rat brain with seed point shown with black marker 62

4-19 Results obtained from analysis of the rat brain with seed point shown with black marker 63

4-20 Depicts the colored FA diagram of healthy rat brain 64

Abstract of Thesis Presented to the Graduate School
of the University of Florida in Partial Fulfillment of the
Requirements for the Degree of Master of Science

PERPENDICULAR FIBER TRACKING FOR FIBER BUNDLE ANALYSIS

By

Siddharth Ray

May 2012

Chair: Walter G. O'Dell
Major: Biomedical Engineering

Diffusion Tensor Imaging (DTI) is a well accepted Magnetic Resonance (MR) imaging technique that can non-invasively analyze the diffusivity patterns of water in neural tissue and visualize neural fiber tracts inside the brain. However, the majority of existing fiber tracking techniques ignores the features of diffusion perpendicular to the individual fiber, which may contain unique information on the local patterns of diffusion. These secondary patterns have not been adopted for clinical use due to a variety of reasons, including high computational demands and high complexity involved in analyzing neural fiber tracking information. In this work I introduce the idea of perpendicular fiber tracking, for neural fiber bundle analysis, and I present a novel dynamic programming method that traces surfaces that are locally perpendicular to axonal fibers. This is achieved by using a cost function with a geometric as well as a fiber orientation term that is evaluated dynamically over the entire image domain starting from a given seed point. The proposed method is validated using synthetic DW-MRI datasets and is then applied to real brain datasets. The results demonstrate the accuracy and effectiveness of our method. The presented technique can be used for fiber bundle segmentation, as a clinical tool for neural fiber analysis, and potentially as a

biomarker for various brain diseases, including Alzheimer's disease, epilepsy, Parkinson's disease. The outcome may also be applied to improve modeling of cancer cell migration.

CHAPTER 1
INTRODUCTION

1.1 Objectives

The long term objective of this project is to provide fiber bundle metrics, using an interactive algorithm for fiber bundle analysis. This algorithm could be used clinically as a biomarker for diagnosing and monitoring atrophy for epilepsy [1], Schizophrenia [2], Alzheimer's diseases [3], Parkinson's Disease (PD) [4] and potentially other dementias, as well as to predict cancer cell migration in the brain [5]. My specific objectives include

- To develop a perpendicular fiber tracking algorithm that computes in real time statistics on variation of the structure, size and curvature along a fiber bundle.
- Validate the method on synthetic data sets with known fiber geometry.
- Demonstrate the technique using real Diffusion Weighted Magnetic Resonance Imaging (DW-MRI) data sets of control (healthy) and diseased (epilepsy) rat brains.

1.2 Clinical Motivation

Each year in United States approximately 1.2 million people aged 18 years and older are newly diagnosed with the onset of brain disease. Approximately 14 million people, or approximately 14% of the population, are impaired with some type of brain disease/disorder [6]. Some of the most common forms of brain disease are: Alzheimer's disease (AD), epilepsy, Parkinson's disease (PD) and brain cancer. Alzheimer's is the most prevalent brain disease and is expected that in the United States alone, there will be approximately 15 million people with AD by 2050 [7]. As of now, AD is largely untreatable and it's causes are unknown although, ageing is considered to be the strongest risk factor. At present, AD is the fifth leading cause of death in the United States and the number of deaths has increased by 66% between 2000 and 2008 [7]. Following AD, epilepsy is the second most common brain disorder, with 250,000 people

diagnosed annually [7]. Epilepsy can often be treated by surgery or medication. However, the development of epilepsy and its progression often cannot be properly diagnosed. Also, epileptic seizures can sometimes have adverse effect on cognition. The next most chronic neurodegenerative disease is Parkinson's disease (PD). On average, the total number of newly diagnosed PD patients is 50,000 annually. At present, PD is not curable and there is no objective, quantitative diagnostic test that can provide clinical efficacy for new treatments.

Although the number of people diagnosed with primary brain cancer is not as many as for AD and epilepsy, cancer is the second leading cause for death in children and males. It has been estimated that in 2012 there will be 64,530 new cases of brain cancer, including 24,070 malignant cases [8]. Some of the more common brain tumors types are: glioblastomas, astrocytomas, oligodendrogliomas and medulloblastomas [9]. At present, treatment for primary brain cancer involves surgery, chemotherapy and/or radiation therapy. Yet the five year survival rate for patient with glioblastoma and of age 45-50 is only 6% and that for anaplastic astrocytoma is 29% [8].

1.3 Current Methods for Diagnosing and Treating Brain Diseases/Disorders

As of now, there is no quantitative and objective method to diagnose and cure dementias. Current methods of diagnosis include standard medical tests, a neurological exam and brain imaging (structural or functional).

The standard group of medical tests includes a blood test for anemia and blood-glucose, a thyroid exam and a liver exam, and are conducted to eliminate other diseases. The standard neurological exam includes checks of reflexes, muscle strength and, eye movement and are performed to detect the type of disorder. Imaging exams

are typically acquired using X-ray, computed tomography (CT) or magnetic resonance imaging (MRI).

The standard of care of treatment includes medication, chemotherapy, radiation therapy and/or surgical resection. An improved method for diagnosing the severity of dementias would enable improved patient-specific selection of treatment procedures.

The U.S. Food and Drug Administration (FDA) has currently approved a class of cholinesterase inhibitors to treat AD. This includes tacrine, donepezil, rivastigmine, and galantamine. However, their common side effects include dizziness, agitation and delusion. Namenda regulates glutamate activity and is also prescribed for people suffering from moderate to severe AD. The treatment regimen for epilepsy depends on the severity, frequency and types of seizure. Carbatrol, zarontin, topamax are the most common first line of treatment for epilepsy. When seizures cannot be controlled by medication, surgery is then considered. For tumors, complete resection is, generally, used as the initial therapy. However, some forms of brain cancer are highly infiltrative and cannot be removed completely with surgery. Radiotherapy is often used to treat the microscopic spread of the cancer around the resection cavity. Temozolomide, BCNU and cisplatin are drugs that are frequently used as complement to surgical resection and radiotherapy.

1.4 Need for Improvement

There is an urgent need for a non invasive structural biomarker to aid in the early diagnosis of brain disease and quantify disease progression. Also, early detection of epilepsy and PD in patients could avert surgical resection, while early diagnosis of AD could change the course of treatment. Finally an improved identification of white matter

tracts could add in the tracking of the migration of tumor cells in brain [5] and thereby may improve the treatment of aggressive brain cancer.

1.5 Organization of Report

The upcoming chapters of the thesis are organized as follows:

Chapter 2 introduces the idea of perpendicular fiber tracking and method that implements it using Dynamic Programming (DP). It describes Diffusion Tensor Imaging (DTI) and tractography, a non-invasive technique to track nerve fibers in white matter. It discusses the criteria used for case selection, DTI acquisition, DTI reconstruction, tractography methods and the algorithm for DP.

Chapter 3 demonstrates the accuracy of the algorithm. The perpendicular fiber tracking method is applied to several synthetic datasets with known fiber geometry. The changes in area and curvature of the perpendicular surfaces/sections, for the synthesized data sets, are then computed and compared with the ground truth.

Chapter 4 depicts the results obtained from a real rat brain DW-MRI dataset. It contains images that show the colored fractional anisotropy (FA) map, cost surfaces at 8-10 locations in different regions of brain and plots of changes in cross sectional area and curvature of the surfaces.

Chapter 5 summarizes the thesis, specifies the scientific and clinical contribution of this work, points out some limitations of the technique. It also discusses the improvements and potential future work.

CHAPTER 2
METHODS

2.1 Background

The overall structural information of axonal fibers in tissue can be acquired by analyzing the primary, secondary and tertiary orientation of fiber bundles using diffusion weighted magnetic resonance imaging. The aim of this study is to trace sections that are locally perpendicular to the axonal fibers. This is achieved by using a cost function with a geometric as well as a fiber orientation term that is evaluated dynamically over the entire image domain starting from a given seed point. As applied to patients, the method is dependent upon diffusion tensor imaging (DTI) datasets and methods to track fiber bundles through the tissue. I will first provide background information for MR-DTI and several of more common tractography algorithms, including deterministic, probabilistic and their combinations.

2.2 Magnetic Resonance Diffusion Tensor Imaging (MR-DTI)

Diffusion-weighted imaging is a magnetic resonance (MR) technique that uses a set of diffusion encoding gradients in addition to imaging gradients (Figure 2-1) to generate the contrast in image due to differences in diffusivity of water molecules in the tissue.

The degree of diffusion weighing depends on the strength of diffusion gradient, the time duration of the gradient pulses and the time separation between them. The cumulative effect of these parameters is expressed using the b-value.

$$\mathbf{b} = \mathbf{G^2\delta^2\gamma^2(\Delta - \delta/3)} \qquad \mathbf{(2.1)}$$

where G – amplitude of the diffusion encoding gradient,

δ – duration of diffusion encoding gradient,

γ – Gyro magnetic ratio and

Δ – time interval between the two diffusion encoding gradients.

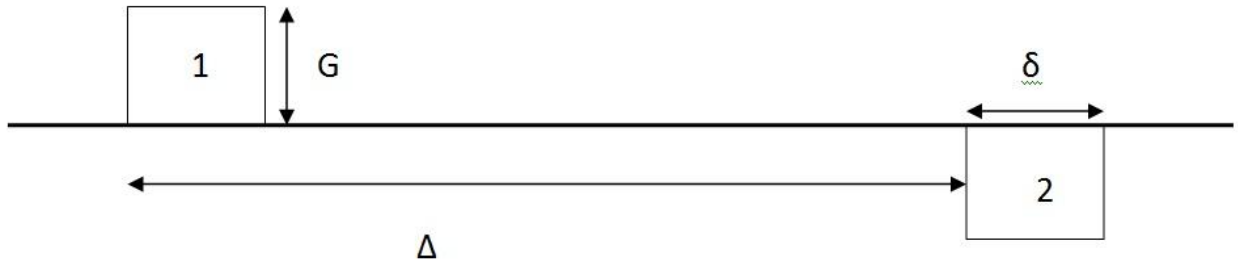

Figure 2-1. Diffusion encoding gradients. The blocks identified as 1 and 2 represent the bipolar diffusion-weighting gradient pulses applied on either side of a 180° radio-frequency excitation pulse (not shown) and are separated by the time interval (Δ). Gradient 1 labels the spins with a phase along the gradient direction (not depicted) and gradient 2 rephases the spins that have not moved. Spins that move along the direction of the applied diffusion gradient accrue a net phase.

The signal strength reduction in DWI is given by the following equation:

$$S = S_0 e^{(-bD)} \qquad (2.2)$$

where S = signal intensity with the diffusion encoding,

S0 = signal without diffusion gradient,

b = b value,

D = Apparent Diffusion Coefficient (ADC).

From the above equation, the signal intensity is low for a high diffusion coefficient.

ADC describes the average diffusion of water molecules in the region of interest, which is usually the two dimensional (2D) pixel or three dimensional (3D) voxel The ADC is sufficient to describe isotropic diffusion. To better understand the anisotropy of diffusion, Peter Basser introduced diffusion tensor imaging (DTI) [10] in 1994. The diffusion tensor is a symmetric matrix with 6 unique values,

$$\begin{bmatrix} D_{xx} & D_{xy} & D_{xz} \\ D_{yx} & D_{yy} & D_{yz} \\ D_{zx} & D_{zy} & D_{zz} \end{bmatrix} with\ D_{yx} = D_{xy},\ D_{zx} = D_{xz}, and\ D_{zy} = D_{yz} \qquad (2.3)$$

In DTI, a data set contain images obtained with different b factors and gradients applied in different directions in addition to an image with no diffusion encoding (i.e. b=0 or B0 image). As the tensor has 6 unique values, a minimum of 6 measurements with different diffusion gradients and one without the diffusion gradient are needed. DTI is generally obtained with more than 6 measurements and is solved to calculate the 6 diffusion coefficients (Dxx, Dxy, Dyy, Dyz, Dzz and Dxz). After computing the coefficients, the tensor may be diagonalized into the three eigenvalues λ1, λ2, λ3 and the corresponding eigenvectors. The vector corresponding to largest eigenvalue, called principal eigenvector, gives the direction of maximal diffusion called the Principal Diffusion Direction (PDD). The relative strengths of the 3 eigenvalues are often graphically represented with a diffusion ellipsoid that describes the directionality as well as magnitude of water diffusion. After calculating the eigen system, the mean diffusivity and Fractional Anisotropy (FA) are calculated as:

$$FA = \sqrt{\frac{3}{2}}\sqrt{\frac{(\lambda_1-\lambda)^2+(\lambda_2-\lambda)^2+(\lambda_3-\lambda)^2}{\lambda_1^2+\lambda_2^2+\lambda_3^2}} \text{ where } \lambda = \frac{\lambda_1+\lambda_2+\lambda_3}{3} \qquad (2.4)$$

The FA value reflects the degree of anisotropy of the diffusion environment. An isotropic diffusion gives an FA value of zero, while an infinitely-strong directional dependence gives an FA of one.

2.3 Fiber Tracking

DTI is a well-established technique used to interpret neural trajectories and to track neural pathways. The principal eigenvector is assumed to be orientated parallel to

the local fiber tract. In the simplest form, mapping the principal eigenvector direction at each voxel forms the basis for tractography – the task of following a connected fiber bundle across many voxels.

2.3.1 Deterministic Tractography

In deterministic tractography, also called streamline tractography, there is a continuous agreement between connected points along the fiber bundle. Tracking starts at a seed point and follows a favored direction until reaches a new measurement (usually the adjacent voxel). The fiber tracking method developed by Basser et al. [11] is one of an illustrative example based on this technique. Basser et. al in [11] represented the fiber tract tractography in 3D space as a curve r(s) parameterized by arc length s. The evolution of r(s) is described with a differential equation.

$$\frac{dr(s)}{ds} = t(s) = \varepsilon_1(r(s))$$

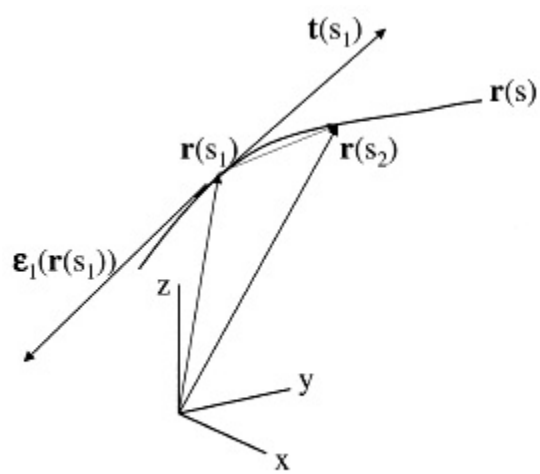

Figure 2-2. Illustration of fiber trajectory. The tangent t(s) identifies the largest eigenvector of tensor D at r(s) (taken from [11]).

The tangent vector is equated to the principal eigenvector for a particular location in the tissue. The vectors in the above equation are computed by using either Euler's

method or the Runge-kutta method. The continuous representation of a tensor field is obtained by using B-spline interpolation function over the 3D grid of voxel-based DTI measurements.

Based on the above formulation, Mori *et al*. [12] introduced Fiber Assignment by Continuous Tracking (FACT). In streamline tractography, Figure 2-3, tracking starts from the seed voxel and tracks to the center of the adjacent voxel in the eigenvector direction. This method restricts the direction of the reconstructed fiber in 26 angle ranges. FACT overcomes this limitation by starting the tracing from within a seed voxel, taking sub-voxel steps along the PDD until the tracing enters a neighbor voxel, and the sub-voxel stepping process continues along the new PDD. In comparison with the original method of Basser, the resultant fiber obtained through FACT deviates less from the underlying fiber bundle in regions of fiber curvature, as shown in Figure 2-3.

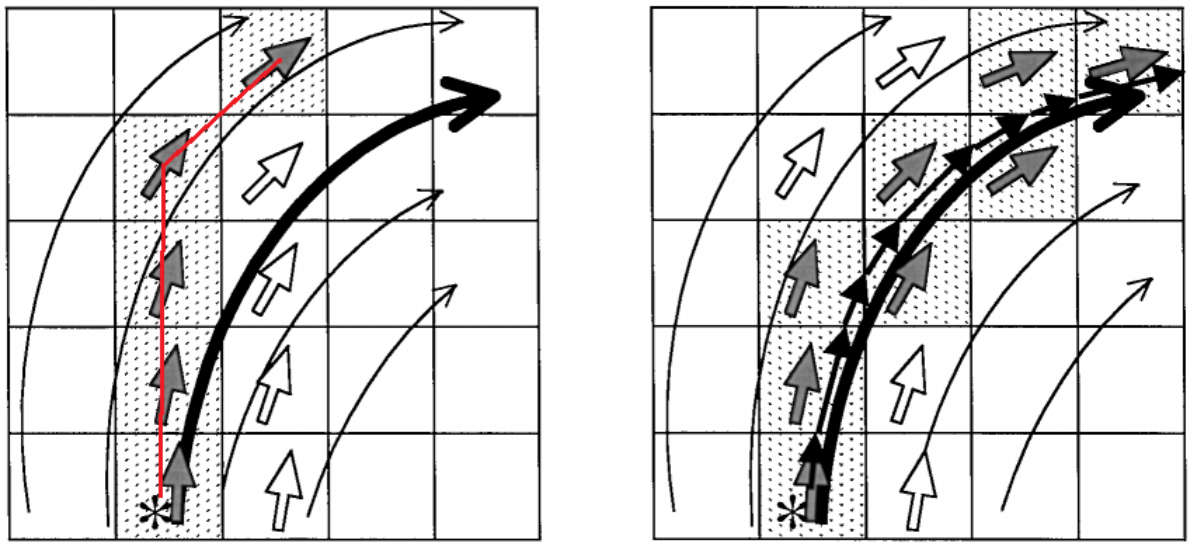

Figure 2-3. Illustration of streamline and Fiber Assignment by Continuous Tracking (FACT) method of tractography. The principal eigenvector in each voxel, assumed for illustration purposes to lie within a two-dimensional plane, is represented by an arrow. The seed voxel is indicated by the asterix in the diagram. In the diagram on the left, the fiber is traced by connecting the center of each voxel towards the direction of eigenvector. While in the diagram on right, tracking starts from the seed voxel, follows the PDD inside

the voxel using sub-voxel steps and continues along the PDD of each traced voxel (taken from[12]).

The computational cost of deterministic tractography is low and output tracts are easy to interpret. However, as calculations are made on local scale, error is accumulated along the tracts as one traces farther from the seed location.

2.3.2 Probabilistic Tractography

In reality, the voxel size of a patient MRI scan is larger than an actual axon and also not every point in brain has only one connection, but can have many. In probabilistic tractography, fiber tracts are computed by drawing a propagation from an underlying model of the distribution fiber orientations, rather than relying directly on the PDDs. The fiber tracking is done repeatedly, thousands of times, each time in a slightly different direction. The set of all the different paths are then collectively analyzed to compute the most highly-probable direction. The method gives a more detailed picture of fiber connectivity in brain and is more robust in complex intra-voxel fiber configurations. However, this approach is computationally costly and the outcome connectivity maps are more difficult to interpret.

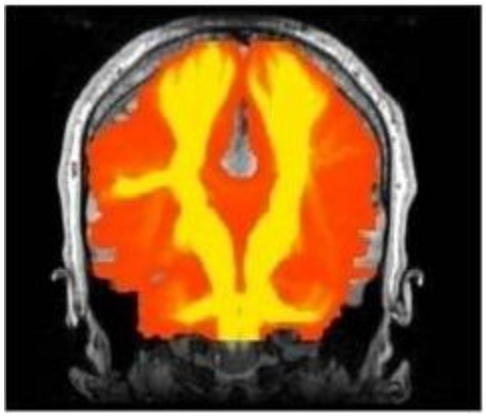

Figure 2-4. Connectivity distribution with seed point in posterior limb (taken from [13]).

2.3.3 Combination of Deterministic and Probabilistic Tractography

To combine the advantages of both approaches, methods to track short fiber tract clusters have been proposed. In [14] a method labeled Split and Merge Tractography (SMT) tracks all of the fiber tracts inside an investigated area while minimizing the total energy. Although using short fiber tracts minimizes the error described for the deterministic approaches, the computational cost is still high. More recently, global energy minimizations based short track fiber clustering algorithms have been proposed [15][16][17]. In these works, short fiber tracts are randomly generated and are allowed to move, rotate and assemble with other fibers to minimize internal and external energies.

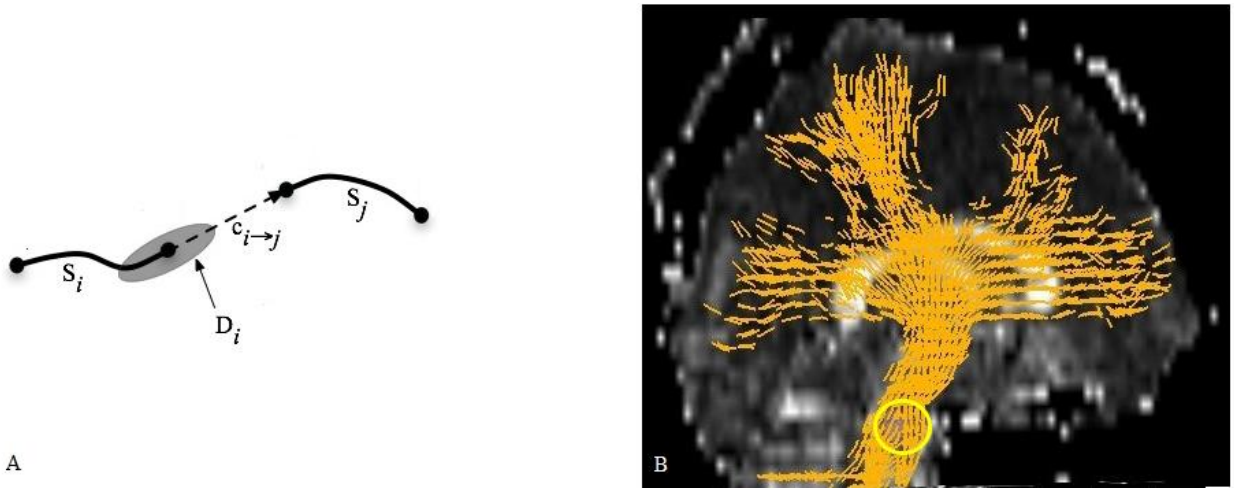

Figure 2-5. Illustration of Split and Merge Tractography (SMT). [A] Two short fibers Si and Sj connected by bridge ci→j that has been selected by Gaussian distribution Di. [B] Shown are short tract clusters for a seed tract starting from the upper brain stem(taken from [14]).

2.4 Method

2.4.1 DTI Reconstruction

After obtaining the MR-DTI data sets, calculations of the diffusion tensor, eigenvectors and FA values for each voxel were done in MATLAB version 2009b. The diffusion data was reconstructed using the fanDTasia toolbox developed by Barmpoutis

et al. at the University of Florida ("Tutorial on Diffusion Tensor MRI using MATLAB"). For each voxel, the principal diffusion direction (PDD) was determined by visualizing the diffusion directions using the plot3 command in MATLAB. The color-coded FA map was generated using the imshow() command in MATLAB.

2.4.2 Perpendicular Fiber Tracking Method Implementation

The perpendicular fiber tracking algorithm was implemented in MATLAB on a Microsoft Windows 7 based laptop with following specification: Intel(R) Core™ i3 CPU M 350 @ 2.27 Ghz, 4 GB RAM.

2.4.3 Fiber Bundle Estimation

The process of extracting parameters from a fiber bundle involves perpendicular fiber tracking and implements it using dynamic programming. Perpendicular fiber tracking reconstructs a perpendicular surface along the fiber bundle. The statistical variation in the cross-sectional area and geometric curvature of the reconstructed surface are then analyzed. The method can be summarized in 4 main steps which were as follows:

- A fiber is traced along a given seed point. Any deterministic fiber tracking method can be used.
- The fiber is segmented in N equal length segments. (N should be an integer)
- For each segment, a surface is reconstructed, that is perpendicular to the fiber bundle. The section is constructed using a 3D cost map that is generated by dynamic programming.
- For every perpendicular section, properties such as curvature and the area of the surface are computed.

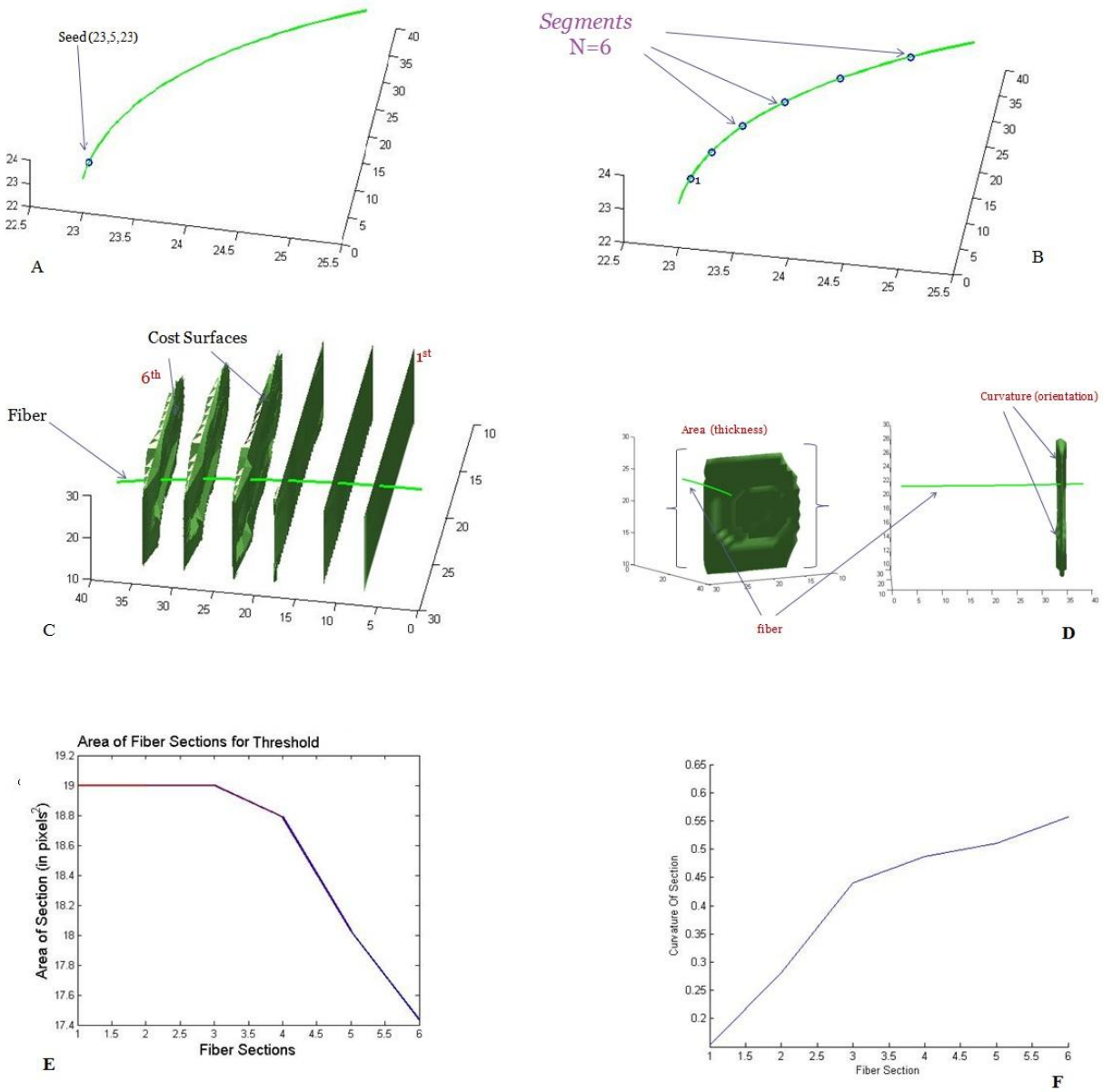

Figure 2-6. Illustration of steps perpendicular fiber tracking. [A] Shown is a fiber traced along seed point, [B] 6 equal length segments along the individual fiber, [C] reconstructed cost surface for all segments, [D] area and curvature interpretation for one of the surfaces, and, [E] and [F] statistics showing variation in area and curvature respectively.

2.4.4 Perpendicular Fiber Tracking

The goal is to reconstructs a 3D surface perpendicular to local fibers within the fiber bundle. The reconstructed surfaces consist of points whose normal vectors are parallel to the principal direction of diffusion of water inside the local fiber. The surface

construction is achieved using a 3D cost map, generated by dynamic programming, that is driven by a cost function of two factors (1) fiber cost and (2) geometric cost.

The 3D cost map maps the total cost of each point in the reconstructed surface. Here, the optimality of the cost map is defined by the minimum total cost for a point from a starting point.

The fiber cost ensures that the section is perpendicular to the dominant local fiber orientation at every point on the surface, while the geometric cost enforces a smoothness and connectivity constraint.

Table 2-1. List the factors and their formulation

Factors	Formulation
Fiber cost	f
Geometric cost	g

2.4.4.1 Geometric cost

The geometric cost ensures the connectivity and smoothness of the perpendicular surface by measuring the parallelism between the vectors of two adjacent voxels. In this work, these vectors refer to the primary eigenvectors and were calculated from the diffusion tensor. The degree of parallelism between two vectors is measured by taking their vector dot product. The geometric cost at a point is given by:

$$g = \varepsilon_s . \varepsilon_r \tag{2.5}$$

where, g - geometric cost,

ε_s - principal eigenvector of seed point and

ε_r - principal eigenvector of neighborhood point

For the case shown in Figure 2-7 where two fibers are parallel, when calculating the geometric cost, all 26 neighboring voxels are considered except the vectors (black) in the voxels just above and below the seed voxel (red vector) that belong to same fiber, 1. So to consider those vectors (colored black) for cost surface reconstruction is not

correct, as the reconstructed section will not be perpendicular to fiber 1 but would reconstruct along the same fiber 1.

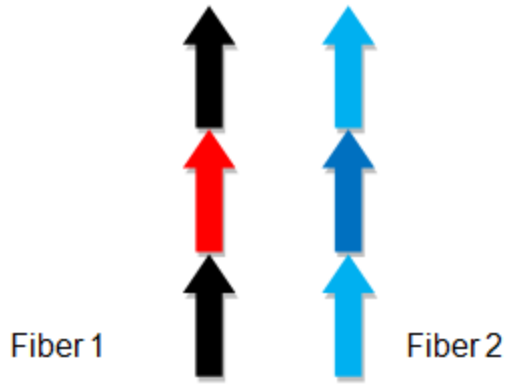

Figure 2-7. Geometric cost. Shown are two parallel fibers 1 and 2. In fiber 1, the seed voxel's unit vector $\mathcal{E}_s$ is colored red and for fiber 2 is colored blue. The voxel unit vector $\mathcal{E}_r$ for which the cost value is to be calculated is dark blue.

2.4.4.2 Fiber cost

The fiber cost ensures that the surface is constructed perpendicular to the fiber bundle. It measures the perpendicularity between the eigenvector of a neighborhood voxel and unit vector, connecting neighborhood voxel to the seed voxel. A less value of dot product of two vectors indicates more perpendicularity between those two vectors.

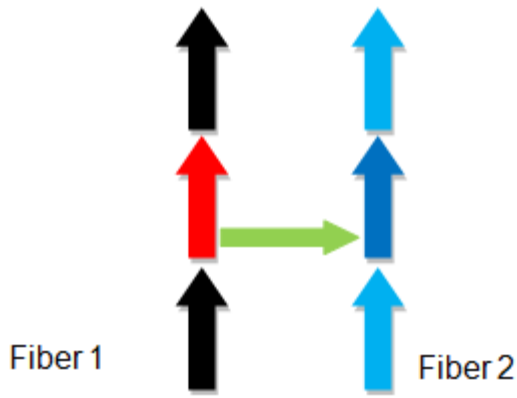

Figure 2-8. Fiber cost. Shown are two fibers 1 and 2. In fiber1, the seed voxel's unit vector is colored red and for fiber 2 is colored blue. The voxel with unit vector $\mathcal{E}r$ for which cost value is to be calculated is dark blue. The unit vector v, colored green, connects the seed voxel to the neighboring vector.

The fiber cost is defined as:

$$f = v.\varepsilon_r \qquad (2.6)$$

where, f - fiber cost,

v - unit vector connecting from seed voxel to neighborhood voxel

$$v = v(s) - v(r)/|v(s) - v(r)| \quad \text{and,}$$

ε_r - eigenvector of neighborhood voxel

For the same above case now shown in Figure 2-8, when considering the 26 neighboring voxels to calculate cost function, the voxel vectors (colored black) just above and below the seed voxel will not be considered, as they belong to same fiber 1. Thus, the surface is constructed perpendicular to local fibers.

2.4.4.3 Total cost function

The total cost function ensures that both the cost functions, fiber and geometric, condition are fulfilled simultaneously. Since both costs should be considered at the same time and a minimum total cost is desired, the geometric cost is subtracted by 1 and is then multiplied by the fiber cost.

$$T = f.(1 - g) \qquad (2.7)$$

2.4.4.4 Thresholds

Calculating the cost for each voxel can require a long execution time. To speed up the analysis, as exclusion cost threshold were predefined for the fiber, geometric and total cost to exclude from future analysis voxels that have a cost value greater than the thresholds. Thus the reconstructed surfaces will only encompass voxels through which the fiber bundle is passing.

2.4.5 Construction of 3D Cost Maps Through Dynamic Programming

The dynamic programming (DP) step was formulated as a graph search for a minimum cost map. The 3D surface reconstruction of the perpendicular section uses a graph search similar to that in [18] but applied in three dimensions.

Figure 2-9 demonstrates the fiber section algorithm realized through DP for a single slice of a 3D image, with the goal to reconstruct a perpendicular section of minimum total cost value. Here we have used a 2D example for a better understanding of the method. Figure 2-9(a) is the initial local cost map with the seed point circled in red (Inf represents a very large number such as 100000 that is used to indicate that a cost has yet to be calculated). In figure 2-9(b) the area around the seed point is expanded (circled grey), showing a portion of the map and cost of pixels where the local total costs are updated for some of the pixels while unchanged for rest of the pixels. The pixels that have higher cost value than the thresholds are not updated. However, the total cost for the pixel can change later, in the algorithm. This can be seen in figure 2-9(c) where the local costs for two points are updated from Inf to 0.8 and 0.9. Figure 2-9(d) and 2-9(e) shows the map at various stage of completion. Figure 2-9(f) depicts the final 2D section reconstructed from the seed point. The surface includes pixels that have a total cost less than the cost threshold, that is here to 1.6. The same methodology is applied on 3D images and yields a 3D cost map.

Inf	Inf	Inf	Inf	Inf	Inf	Inf	Inf	Inf
Inf	Inf	Inf	Inf	Inf	Inf	Inf	Inf	Inf
Inf	Inf	Inf	Inf	Inf	Inf	Inf	Inf	Inf
Inf	Inf	Inf	Inf	Inf	Inf	Inf	Inf	Inf
Inf	Inf	Inf	Inf	Inf	Inf	Inf	Inf	Inf
Inf	Inf	Inf	0	Inf	Inf	Inf	Inf	Inf
Inf	Inf	Inf	Inf	Inf	Inf	Inf	Inf	Inf
Inf	Inf	Inf	Inf	Inf	Inf	Inf	Inf	Inf
Inf	Inf	Inf	Inf	Inf	Inf	Inf	Inf	Inf

(a)

Inf	Inf	0.5
0.4	0	Inf
0.7	0.8	Inf

(b)

0.9	0.8	0.6	0.5
0.7	0.4	0	Inf
0.9	0.6	0.8	Inf

(c)

Inf	Inf	1.1	0.9	0.8
0.9	0.8	0.6	0.5	0.9
0.7	0.4	0	0.8	1
0.9	0.6	0.8	Inf	Inf

(d)

Inf	Inf	Inf	Inf	Inf	1.5	Inf	Inf
Inf	Inf	Inf	Inf	1.4	1.3	Inf	Inf
Inf	Inf	1.3	1.2	1	1.1	Inf	Inf
Inf	1.4	1.3	1.1	0.9	0.8	Inf	Inf
Inf	0.9	0.8	0.6	0.5	0.9	Inf	Inf
Inf	0.7	0.4	0	0.8	1	Inf	Inf
Inf	0.9	0.6	0.8	1.2	1.4	Inf	Inf
Inf	1.3	1.4	1.4	1.4	Inf	Inf	Inf
Inf	Inf	Inf	Inf	Inf	Inf	Inf	Inf

(e)

					1.5
				1.4	1.3
		1.3	1.2	1	1.1
	1.4	1.3	1.1	0.9	0.8
	0.9	0.8	0.6	0.5	0.9
	0.7	0.4	0	0.8	1
1.5	0.9	0.6	0.8	1.2	1.4
1.5	1.3	1.4	1.4	1.4	

(f)

Figure 2-9. Depiction of the dynamic programming approach. (a) Shown is a map of the initial local total cost for each point on the graph and where the seed point has an initial value zero. (b) The region around the seed point (circled gray) is expanded. (c) The region around the first 2 points (circled gray) is expanded. (d) The region around the first 3 points (circled gray) is expanded. (e) Shown is the final local cost matrix after computing local total cost for each point. (f) Shown is the final reconstructed cost matrix, expanded around the selected points. {total cost threshold is 1.6}

2.4.6 Algorithm: Pseudocode for 3D DP for Perpendicular Fiber Tracking

```
Input:
 s                    {start voxel}
 g_th, f_th, T_th      {thresholds}
 Ɛ                    {eigenvectors list}

Data Structure:
L          {List of active voxels sorted initially empty}
N          {Neighborhood set of active voxels (contains 26 neighbors of each voxel)}

Ouput:
C          {Matrix of total cost value for every voxel}

Algorithm:
C←inf;
C(s)←0;   L←s;       {Set seed point cost value to 0 and initialize the active list with seed
voxel}
While L≠ø do begin  {If the list is not empty}
  p←argmin(L); L← L-p;   {Find out the location of minimum cost and remove it}
  for each r ∈ N(p)
      f= Ɛ.(p)×Ɛ(r);       {Compute fiber cost for each neighborhood voxel}
      g= Ɛ(p)×Ɛ(r);        {Compute geometric cost}
        if g<g_th && f<f_th then    {Remove higher cost neighbor}
           newcost ← C(p)+(1-g)*f;       {Compute total cost}
           if newcost < C(r) && newcost < T_th then
               C(r) ← newcost;                    {Assign neighbor total cost}
               L ← L+r;                  {Add it to active list}
         end
      end
  end
end
```

CHAPTER 3
TOWARDS VERIFICATION OF PERPENDICULAR FIBER TRACKING

3.1 Validation on Synthetic Datasets

The main objective of this thesis work is to study the differences in the structure of fiber bundles between normal and disease brains. The algorithm computes the area and curvature of each fiber bundle from the reconstructed 3D section, perpendicular to the local dominant fiber orientation.

To the best of our knowledge there is no prior literature on perpendicular fiber tracking and thus this approach requires a thorough validation. As the exact geometry of real brain datasets are not known, synthetic datasets of different structure with known fiber geometry were used to test the accuracy of the algorithm.

3.2 Generation of Synthetic Dataset

Dr. Barmpoutis helped in synthesizing the DW-MRI datasets using his free, open source Tutorial (http://www.cise.ufl.edu/~abarmpou/lab/fanDTasia/tutorial.php, “Tutorial on Diffusion Tensor MRI using MATLAB”). The datasets simulated fiber bundles with a variety of different fiber structures such as splaying, crossing and furcating. The simulation output is a series of simulated MR images representing a typical DW-MRI exam but where the fiber orientation is specified *a priori* at each voxel and dictates the output DW images.

3.3 Implementation

The generation of synthetic data was implemented using MATLAB software version 2009b. The datasets were generated of different matrix sizes. It took 30-50 seconds to generate a typical data set on a Microsoft Windows 7 based laptop with the following specification: Intel(R) Core™ i3 CPU M 350 @ 2.27 Ghz, 4 GB RAM.

3.4 Specifications

All of the datasets that were created consisted of a series of 22 images, representing different b-values and gradient orientations. The first image corresponded to a low diffusion weighting (S0) and the remaining 21 images had a b-value of 1500s/mm^2 and a unique gradient direction.

3.5 Data Set 1: Inclined Fibers

The first DW-MRI dataset was created by simulating a single fiber bundle with straight fibers inclined at 45° angle from x-axis. The matrix size of this dataset was 21×21×10. As the fibers were straight and linear, the ground truth curvature of the dataset was zero and area was constant throughout the fiber bundle. This is reflected in Figure 3-1 which shows that the curvature of all the segmented points is zero while the area of the cost surface remains constant for the segmented points, which agrees with the ground truth.

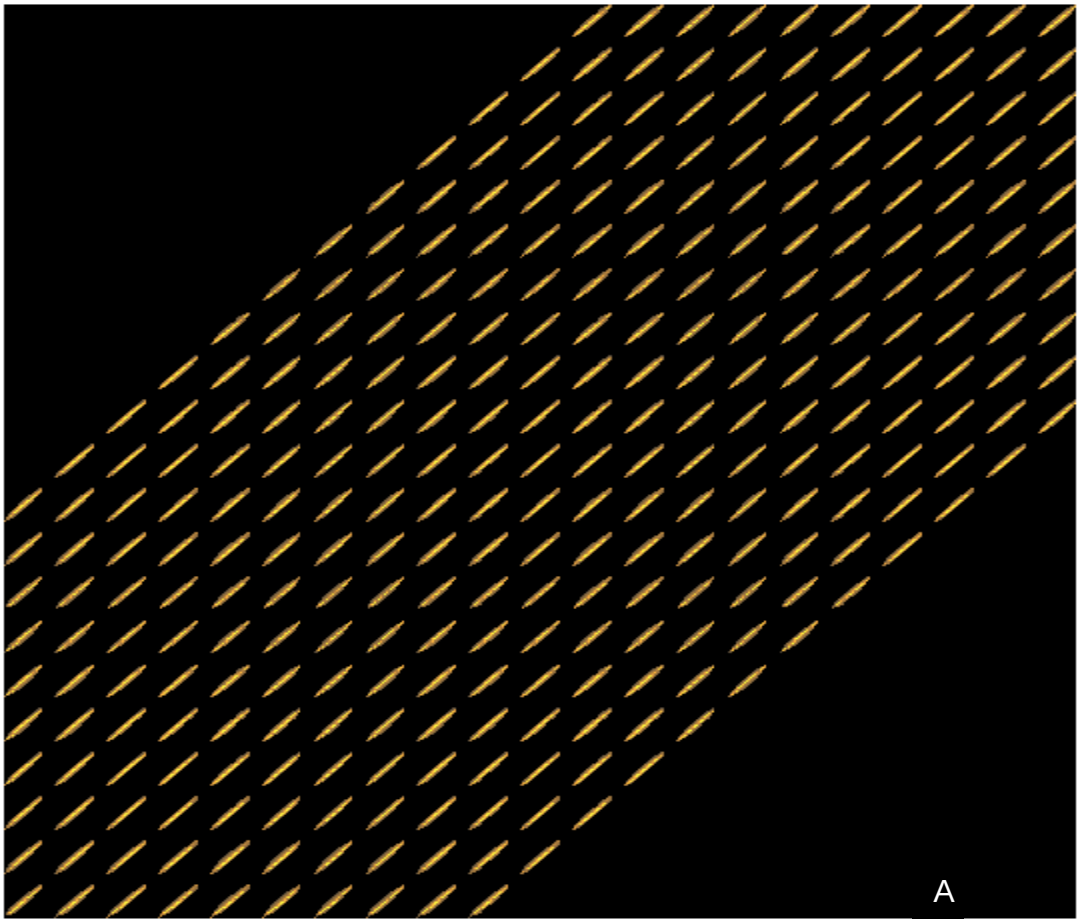
A

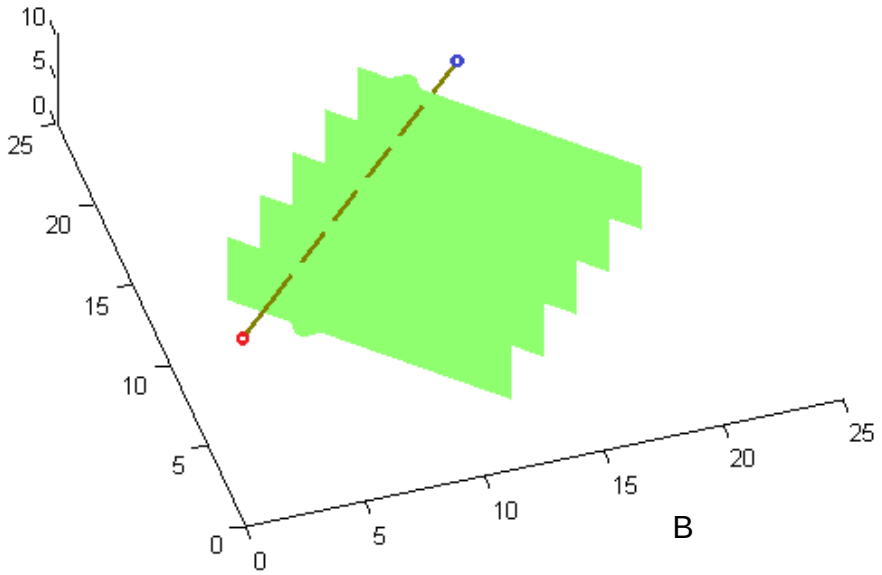
10
5
0
25
20
15
10
5
0
0
5
10
15
20
25
B

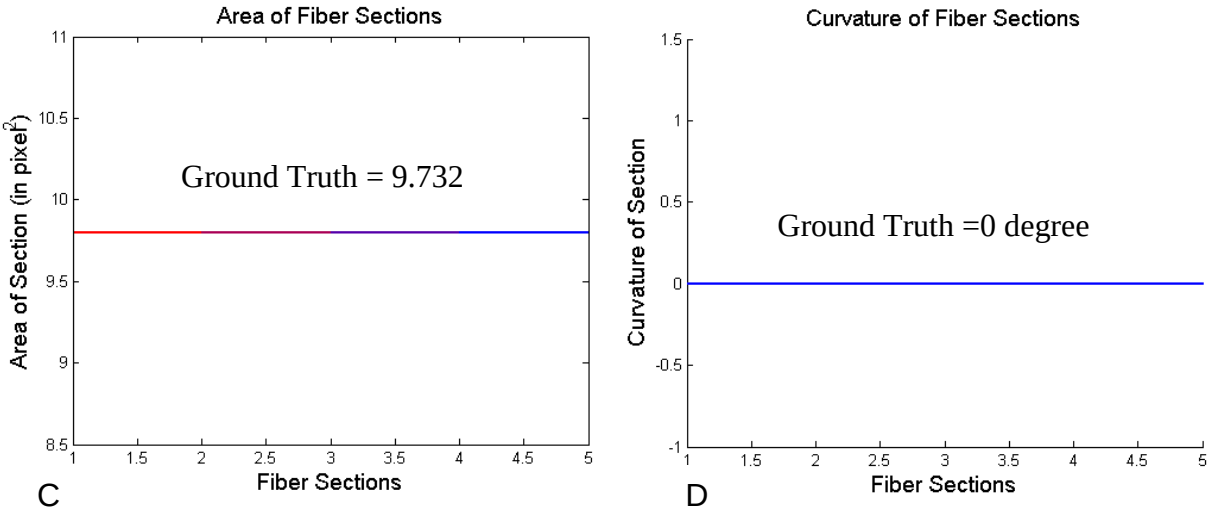

Figure 3-1. Results from synthetic dataset#1: inclined straight fibers. The plot on the top [A] demonstrates the ellipsoidal representation of eigenvectors at each voxel for synthetic dataset#1. [B] The cost surface is depicted at 5 different locations along the fiber bundle and an individual fiber is traced from a seed point (marked in red). The number of fibers remains constant and straight along the length of the bundle from the seed point (red) to the end point (blue). [C] The change in the cross sectional area determined from the algorithm is plotted using red-blue color graded curve. The red-to-blue gradation indicates the distance along the fiber segment, increasing from seed location to the end location. The plot remains constant as the number of fibers remains constant. [D] The plot of curvature remains zero throughout because the fibers were all parallel and bundle was straight.

3.6 Data Set 2: Conical Bundle with Parallel Fibers

The second DW-MRI dataset was created by simulating a single fiber bundle with straight fibers, and a linearly increasing cross sectional area. The matrix size of the dataset was 60*60*60. As the fibers were all straight, the ground truth curvature of the perpendicular section was zero throughout the bundle. Figure 3-1 demonstrates the accuracy of the algorithm. The area of the surfaces increases linearlyalong the fiber, which agrees with the ground truth and the curvature of the surface is zero, which also agrees with the ground truth.

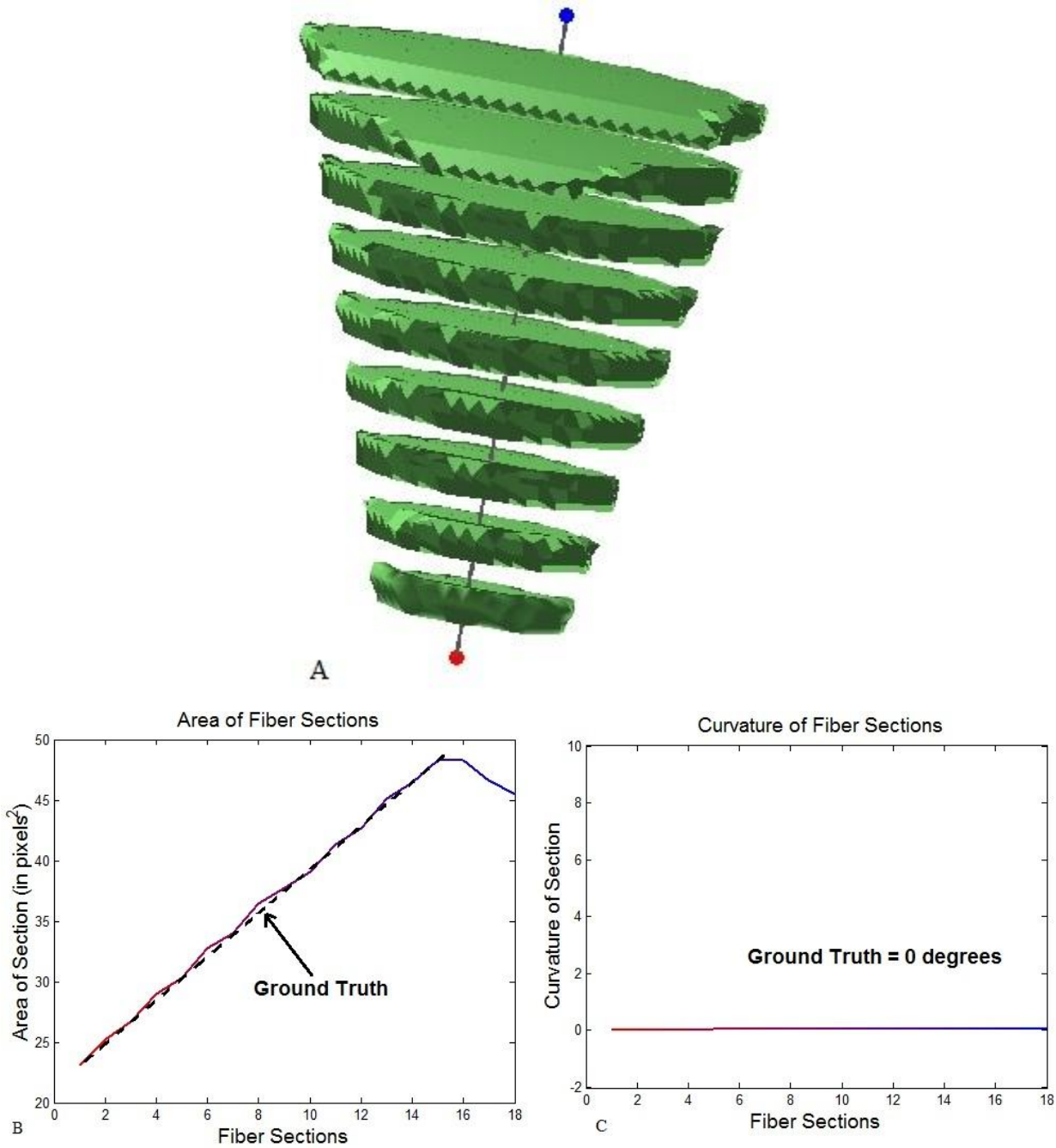

Figure 3-2. Results from synthetic dataset#2: conical bundle with parallel fibers. [A] The cost surface is depicted at 9 different segment locations along the length of the bundle (although there are really 18 sections). The number of fibers and the corresponding bundle cross-sectional area, increase linearly along the bundle from the seed point (marker red) to end point (marked blue). The number of fibers increases linearly and so the section width also increases. [B] The change in area is plotted using red-blue gradation scale. The ground truth is indicated by the straight, dashed line and the algorithm's output matches it well. The plot decreases after 16th location because the dataset reached to the edge of the imaging matrix and is a result of artifact at the

edges. [C] The plot of the curvature remains zero throughout because fibers were all parallel and bundle was straight.

3.7 Data Set 3: Linear and Curving Fibers

The third dataset was synthesized by simulating 2 fiber bundles, one with straight fibers oriented along the z-axis (out of the plane of the paper) inside a cylinder, and the second bundle with circularly-oriented fibers outside the cylinder and with the number of fibers increasing with radius(Figure 3-3). The dataset created was of matrix size 21×15×10. As the fibers, inside the cylinder were all straight and linear (along z-axis), the cross sectional area and curvature remained constant and zero along the segmented location of the fiber bundle. While fibers outside the cylinder area increased in numbers with radius, the cross-sectional area and the curvature of the bundle increased as we move away from the center.

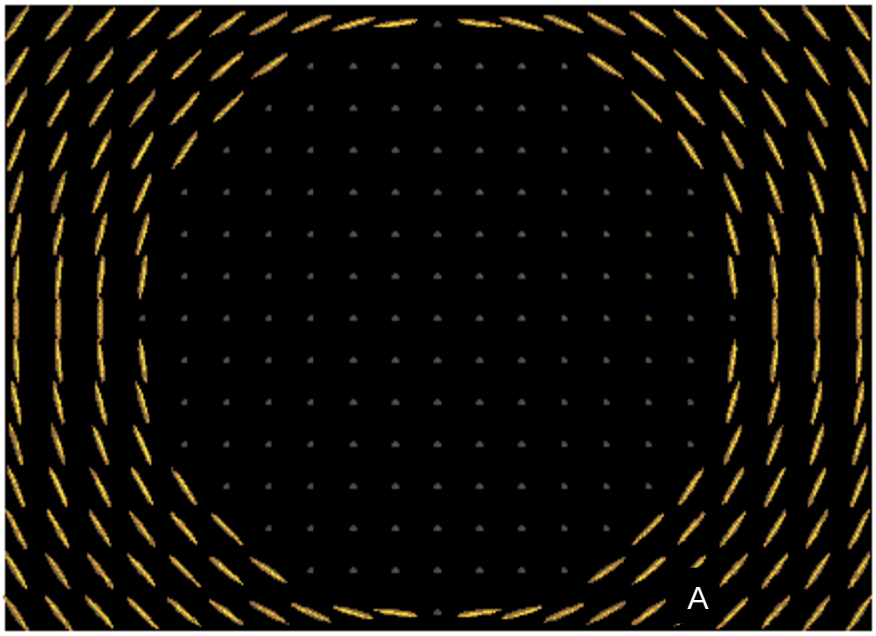

Figure 3-3. Ellipsoidal representation of eigenvectors for dataset#3.

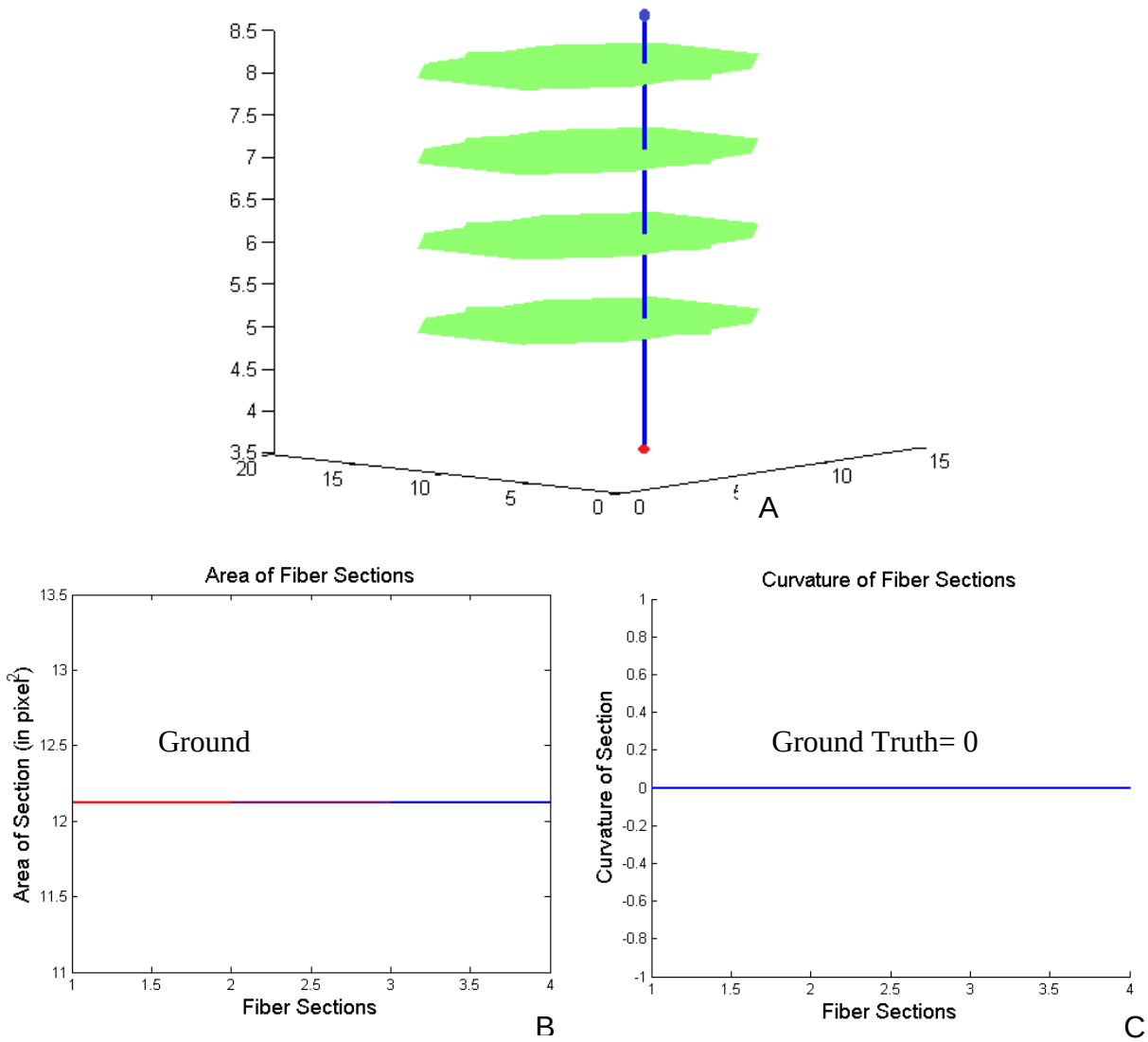

Figure 3-4. Results from synthetic dataset#3: linear and curving fibers. [A] The circular cost surface is depicted at 4 different segment locations along the length of the bundle (inside the cylindrical region). The number of fibers, and the corresponding bundle cross-sectional area, remains constant along the bundle from the seed point (marker red) to end point (marked blue). [B] The change in area is plotted using the red-blue gradation scale. The cross sectional area remains constant along the bundle as all fiber were parallel and straight inside the bundle. [C] The plot of the curvature remains zero throughout because fibers were all parallel and bundle was straight.

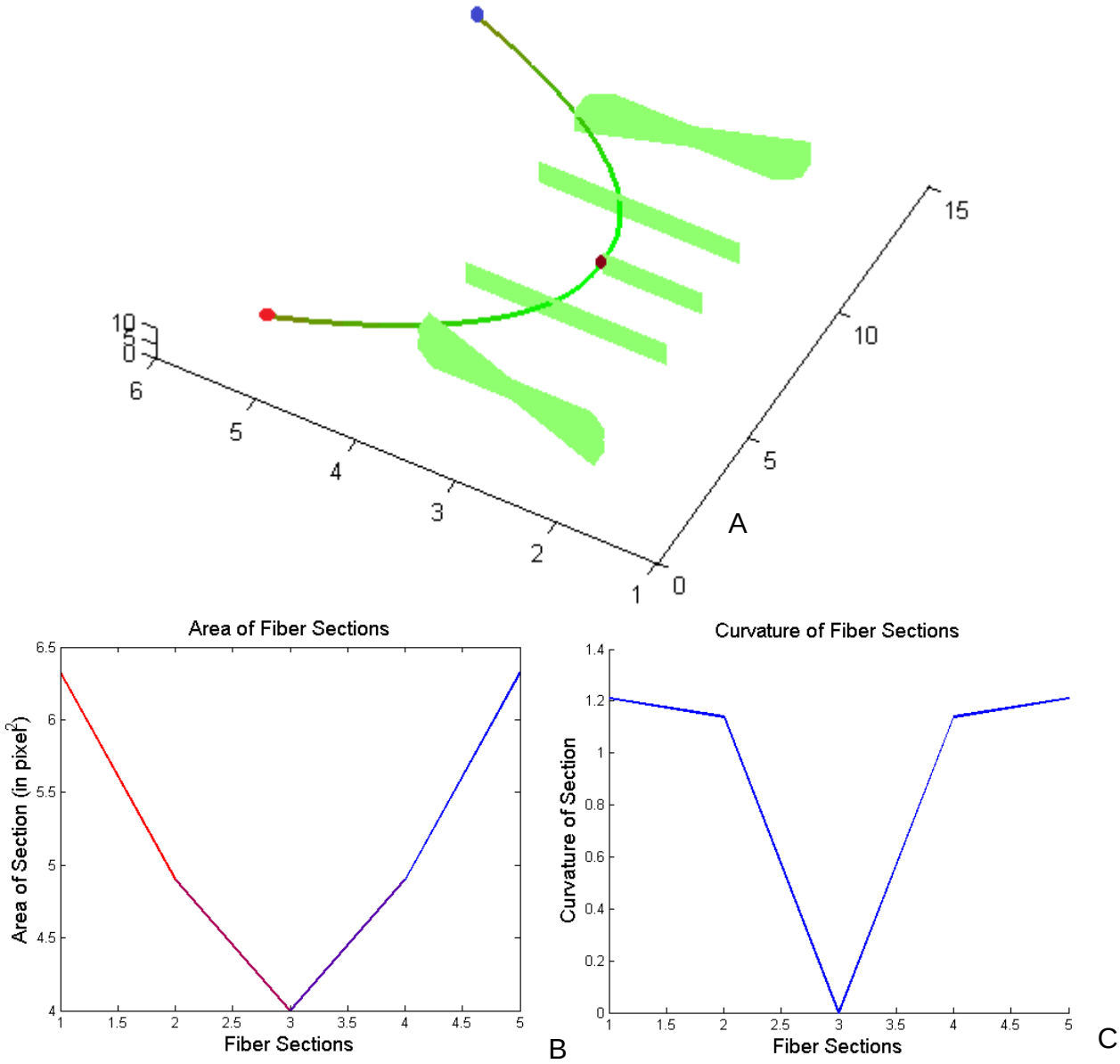

Figure 3-5. Results from synthetic dataset#3: linear and curving fibers. [A] The cost surface is depicted at 5 different segment locations along the length of the bundle (outside the cylindrical region). The number of fibers and the corresponding bundle cross sectional area increases along the bundle from mid point (marked brown) to the seed point (marked red) and end point (marked blue). [B] The change in area is plotted using the red-blue gradation scale. The cross sectional area increases non-linearly along the bundle as the number of fibers increases at extremes (start and end point). [C] The plot of the curvature also increases from the mid-point to the start and end points because the fibers are parallel in the middle region and are curving more along the corners.

3.8 Data Set 4: Fibers Branching

The fourth synthetic dataset was synthesized by simulating a fiber bundle with splaying fibers in a 2D plane, and then extruding this geometry upwards through the entire image stack. The data set was of in-plane matrix size 21×14 and with 10 extruded slices. The fibers were constructed as two cylinders, each with inner radius of 9 pixels and outer radius 13 pixels. Since the centers for the cylinders were (0,0) and (22,0), they shared a common region initially which split as you move upwards along the fibers (Figure 3-6).

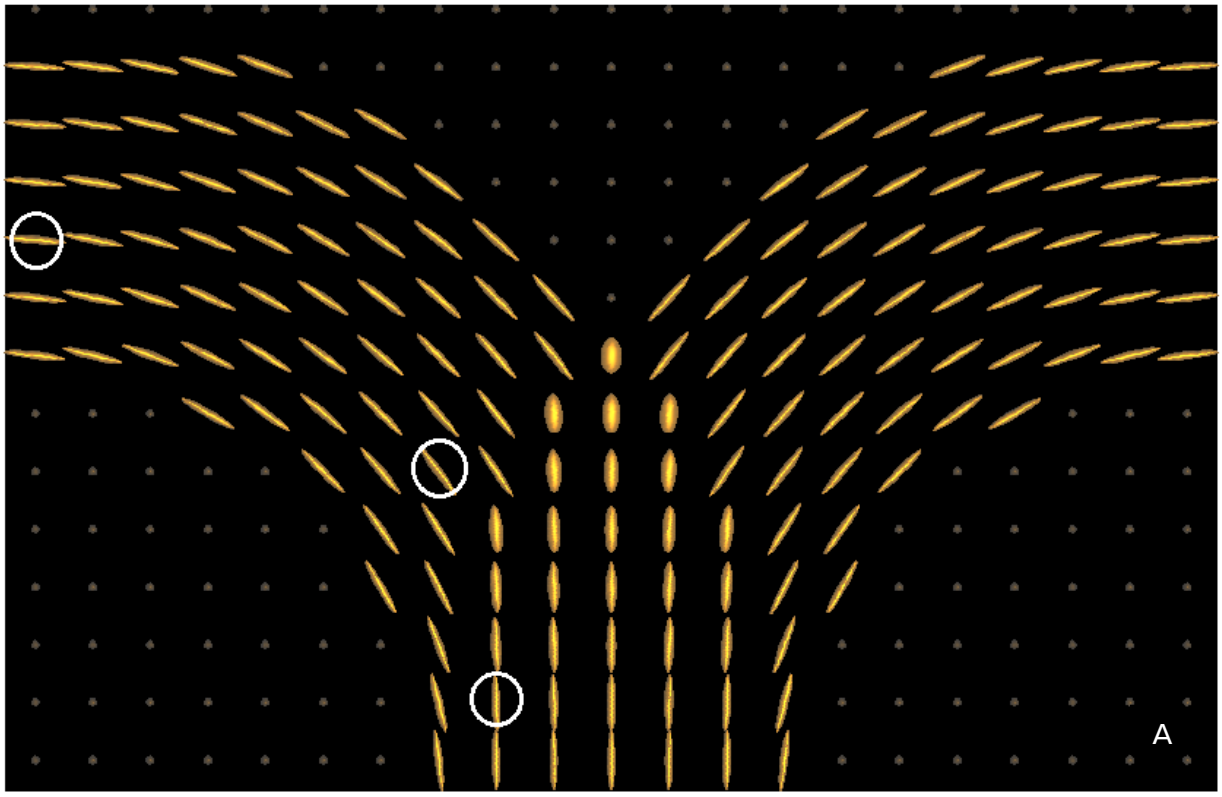

Figure 3-6. Ellipsoidal representation for eigenvectors of fibers branching in synthetic datasets#4. The bubbles get wider approaching the bifurcation as the FA value decreases due to the two different pathways. The fiber bundle area and curvature increases until the branching, and decreases after the branching, because the fibers initially, at bottom, starts splaying in both the directions and the cost surface tends to include all. The curvature again decreases after branching, as fibers get aligned horizontally while the area remains constant after branching. Each segmented locations are marked in white circles.

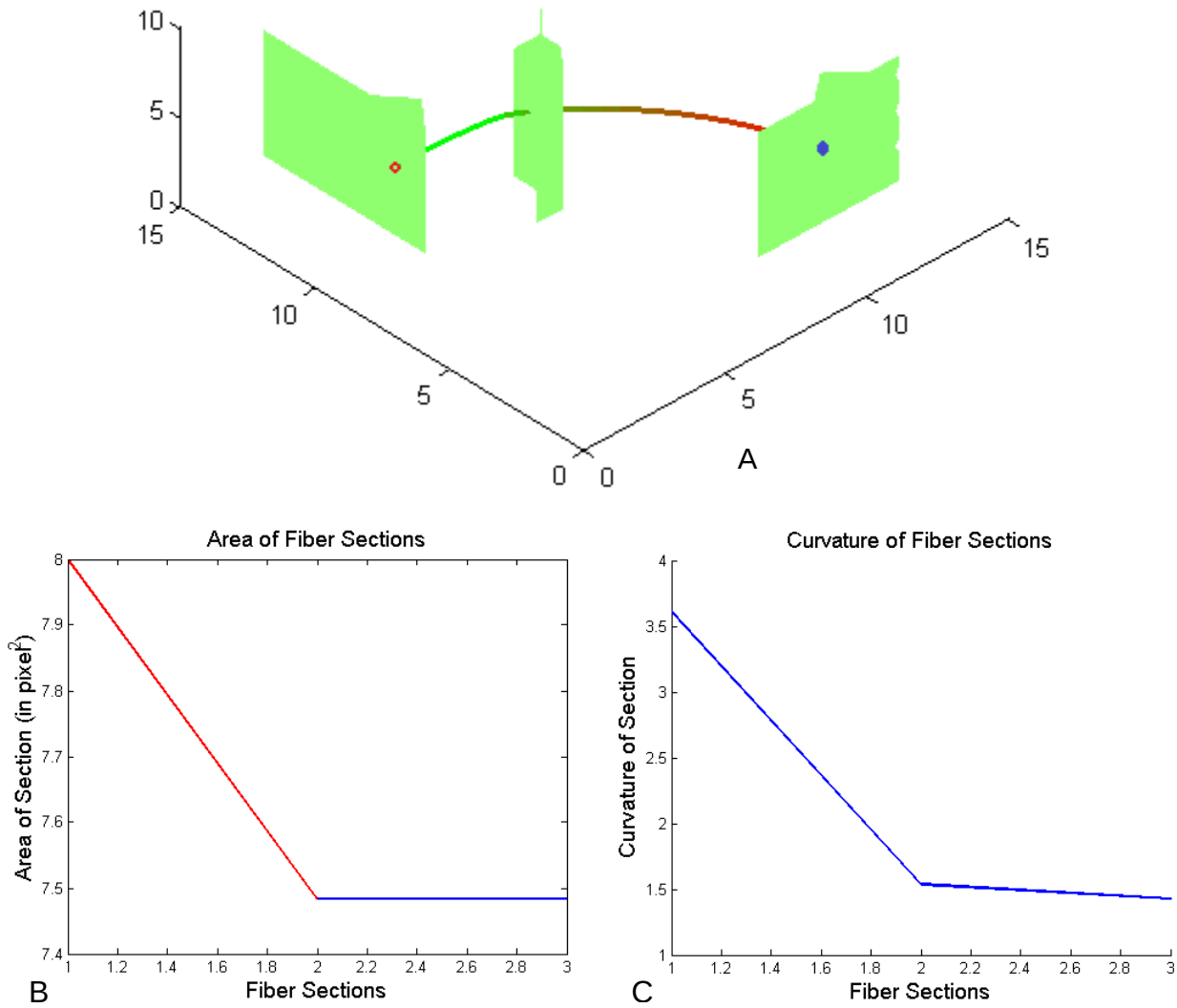

Figure 3-7. Results from synthetic dataset#4: branching fibers. [A] The cost surface is depicted at 3 different locations along the length of the bundle. The number of fibers and the corresponding bundle cross sectional area, decreases, suddenly, after the branching and remains constant afterwards. [B] The change in area is plotted using the red-blue gradation scale. The cross sectional area, first decreases along the bundle as the number of fibers suddenly decreases after the branching, and remains constant afterwards. [C] The plot of the curvature also decreases suddenly after branching, because the fibers are parallel in the middle region and are curving more along the corners.

CHAPTER 4
RESULTS

4.1 Application on Real Datasets

After validating the algorithm on synthetic data, we then applied it on a real rat brain datasets to examine its clinical viability. Cost surfaces/sections were reconstructed at 8 and10 different locations in two different regions (stratum lacunosum-moleculare and stratum oriens) of the rat hippocampus.

4.2 Implementation

The results for the rat brain datasets were obtained using MATLAB version 2009b. The experiments are performed on a Microsoft Windows 7 based laptop with the following specification: Intel(R) Core™ i3 CPU M 350 @ 2.27 Ghz, 4 GB RAM. With these specifications, it took < 2 seconds to generate the cost surfaces and plots of area and curvature for a typical bundle.

4.3 Pre-processing

All images were first filtered using a moving average operator. The filtering operation was performed for a single slice at a time and using a 3×3 averaging kernel.

Additional noise elimination was done with the help of the *surf* command in MATLAB. Command *surf* creates a 3D shaded surface, where the color is proportional to the height. The height of the 3D surface, here, corresponds to the strength of DWI image signal at each pixel at that particular slice. The unwanted signal, the noise, outside the brain region can be easily detected by observing the plot and then the undesirable noise can be cut-off by using *surf*(S(:,:,m,:),t). Here, S is signal obtained from the data set, of size 4D matrix, m is the slice number and t is the threshold by which the signal is cut off. Figure 4-1 shows the use of the above command with S of

matrix size 90×90×56×24 (see 4.4.1 for details), where there are 60 slices of size 94×90 pixels taken in 24 gradient directions, m is taken as 28 and t=8, which means the base line is shifted to 8 (Figure 4-1B). Now for calculating the DTI coefficients, we consider only those signals that have intensity greater than 8. The procedure not only eliminates the noise but also reduces the time to calculate DTI (From eq. 2.2). Figure 4-1 demonstrates this use of *surf*.

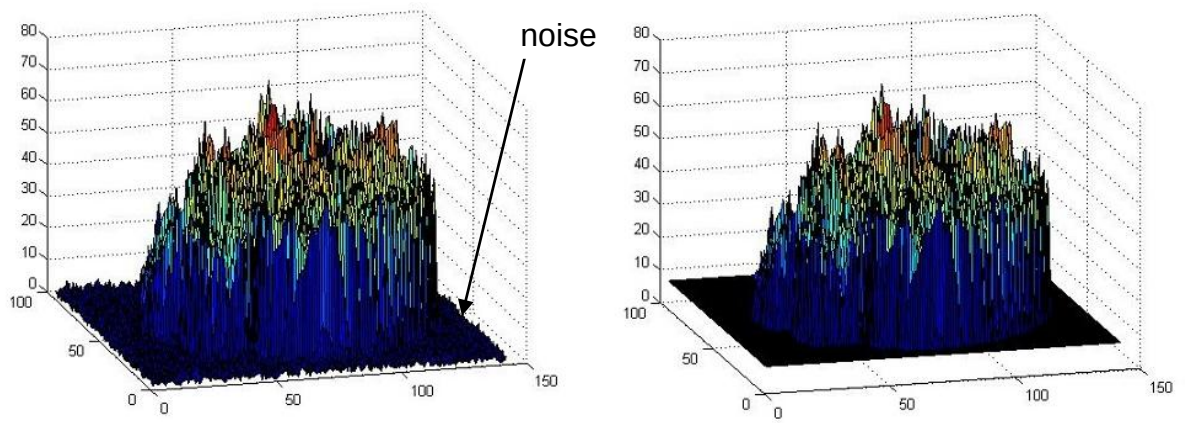

Figure 4-1. Surf plots of a rat brain DWI dataset. The plot on the left shows the signal intensity before setting threshold, the disturbances around the image signal can be seen. The plot on the right shows signal intensity after setting threshold level to 8, almost all noise in the signal are removed.

4.4 Rat Hippocampus

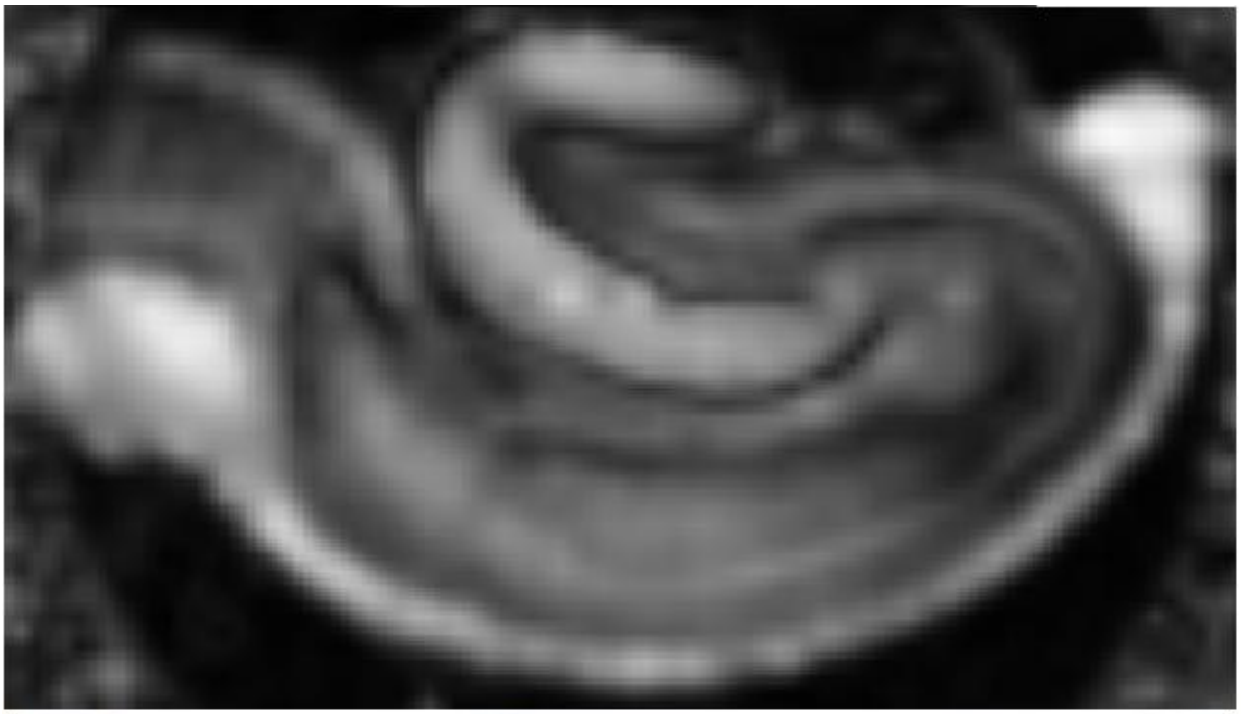

Figure 4-2. Shown is the FA map of the 28th slice out of 56 slices of a representative rat dataset. Shown is s sagittal view through the hippocampus.

4.4.1 Data Acquisition

The acquisition protocol included 56 images using a pulsed gradient spin echo pulse sequence with repetition time (TR) =1.5s, echo time (TE) =28.3 ms, bandwidth =35 kHz, field of view (FOV) =4.5 x 4.5 mm, imaging matrix =90 x 90 with 20–30 continuous 200- micron axial slices. After the first image set was collected with no diffusion weighting (b~0 s/mm), 21 diffusion-weighted image sets with gradient strength (G) = 415 mT/m, gradient duration delta (δ) = 2.4 ms, gradient separation Delta (Δ) =17.8 ms, and diffusion time T-delta (Tδ) = 17 ms were collected. The reader is referred to Figure 2.1 for a schematic of these parameters. These parameters create a b-value of approximately 1250s/mm^2. Each of these image sets used a different diffusion gradient direction whose orientations were determined from the second order

tessellation of an icosahedron projected onto the surface of a unit hemisphere. The image without diffusion weighting had 36 signal averages (time =81 min), and each diffusion-weighted image had 12 averages (time = 27 min per diffusion gradient orientation) to give a total imaging time of 10.8 hours per hippocampus. The temperature was maintained at 20 ± 0.2°C throughout the experiments using the temperature control unit of magnet previously calibrated by methanol spectroscopy [19].

4.4.2 Fiber Bundle Analysis Using Perpendicular Fiber Tracking

The algorithm was performed at two regions on the rat hippocampus dataset. The first one was at the stratum lacunosum-moleculare (Figure 4-3A) and the second one at the stratum oriens (Figure 4-4A). In each run, a primary fiber was defined as starting from a manually-selected seed point and traced through the brain using deterministic tractography, and 8-10 cost surfaces were constructed along the length of the primary fiber. All of the fibers passing along the cost surfaces were traced to ensure that the surfaces did not include the fibers outside the bundle region. The output, fiber sections/surfaces, plot of area of each surface and curvature of each surface, obtained from the algorithm are demonstrated in Figure 4-3.

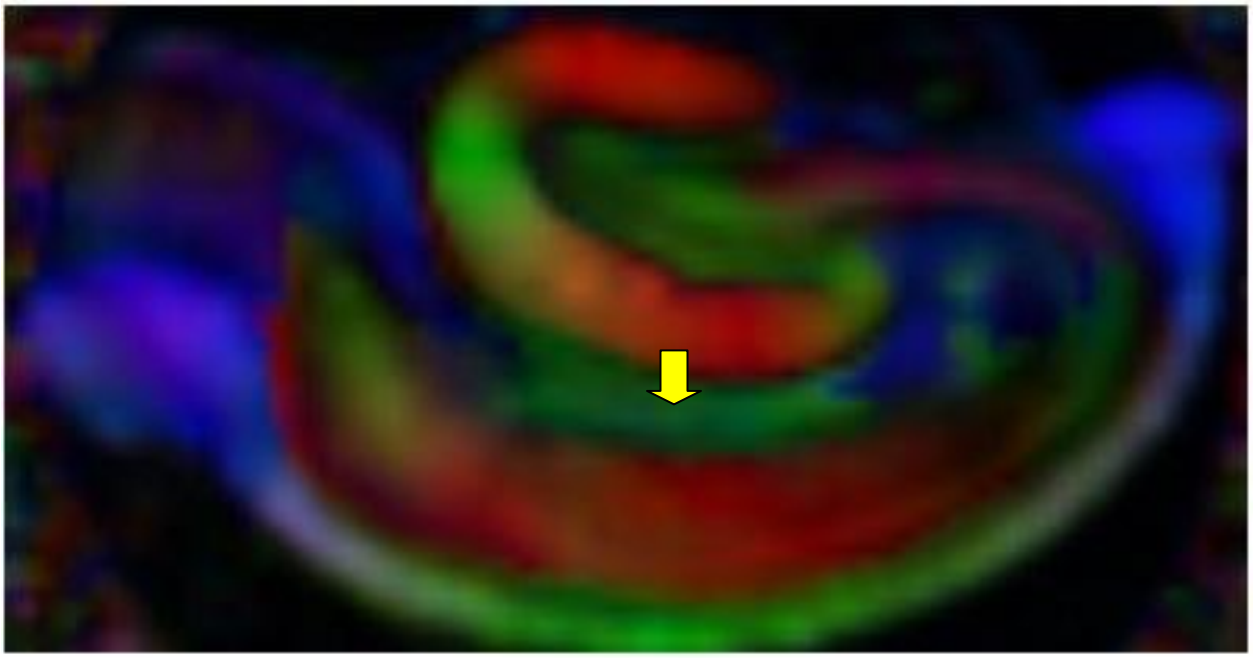

A

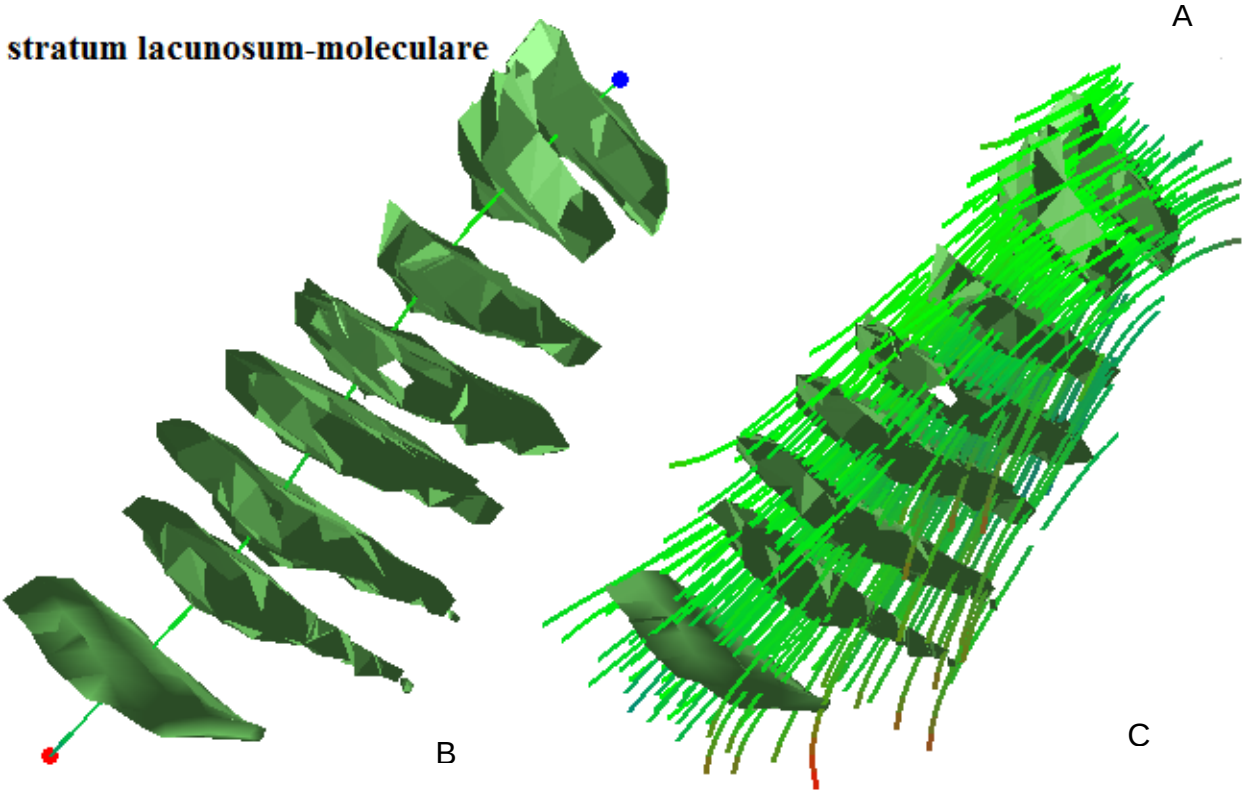

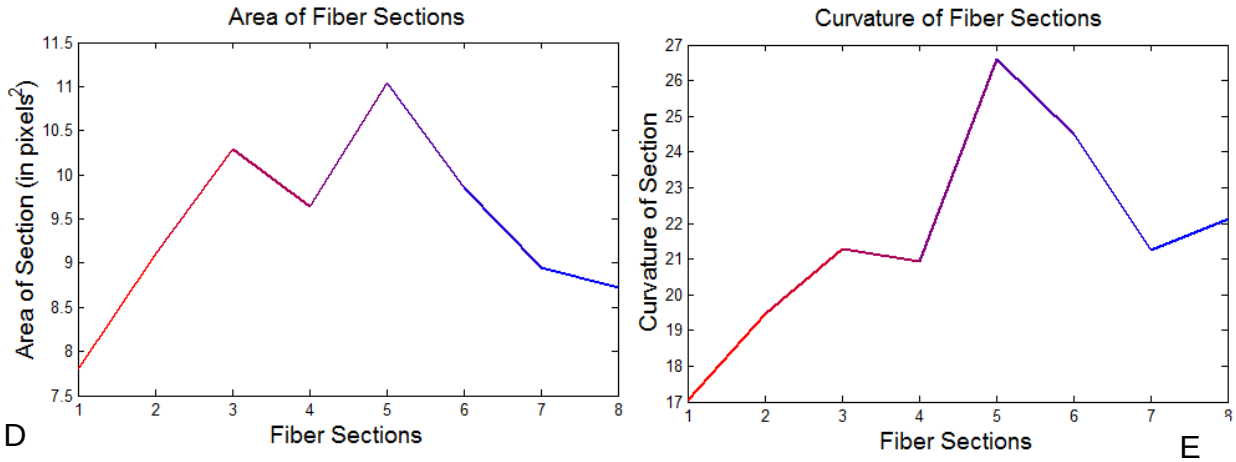

Figure 4-3. Results obtained from analysis of the rat hippocampus with seed point in the stratum lacunosum-moleculare: [A] Shown is the colored FA map where the green, red and blue color indicate the direction of the underlying fibers being the horizontal, vertical or perpendicular (out of plane) respectively. The approximate location of the seed point within the stratum lacunosum-moleculare is indicated by the yellow arrow. [B] The primary fiber was traced from the seed point (marked in red) and cost surfaces were computed at 8 different locations along the length of the primary fiber, from the seed point to the end point (blue). [C] The whole fiber bundle is depicted. [D] and [E] The change in the cross-sectional area and curvature determined from the algorithm is plotted using the red-blue color graded curve. The red-to-blue gradation indicates the distance along the fiber from the seed location to the end location.

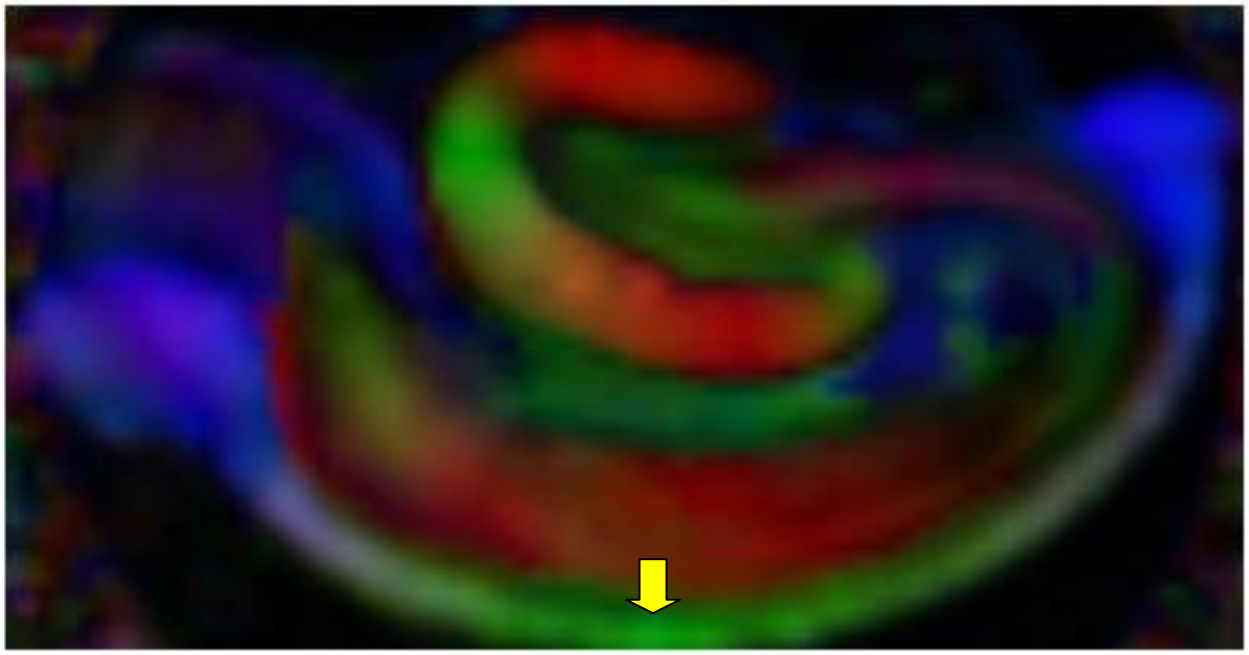

A

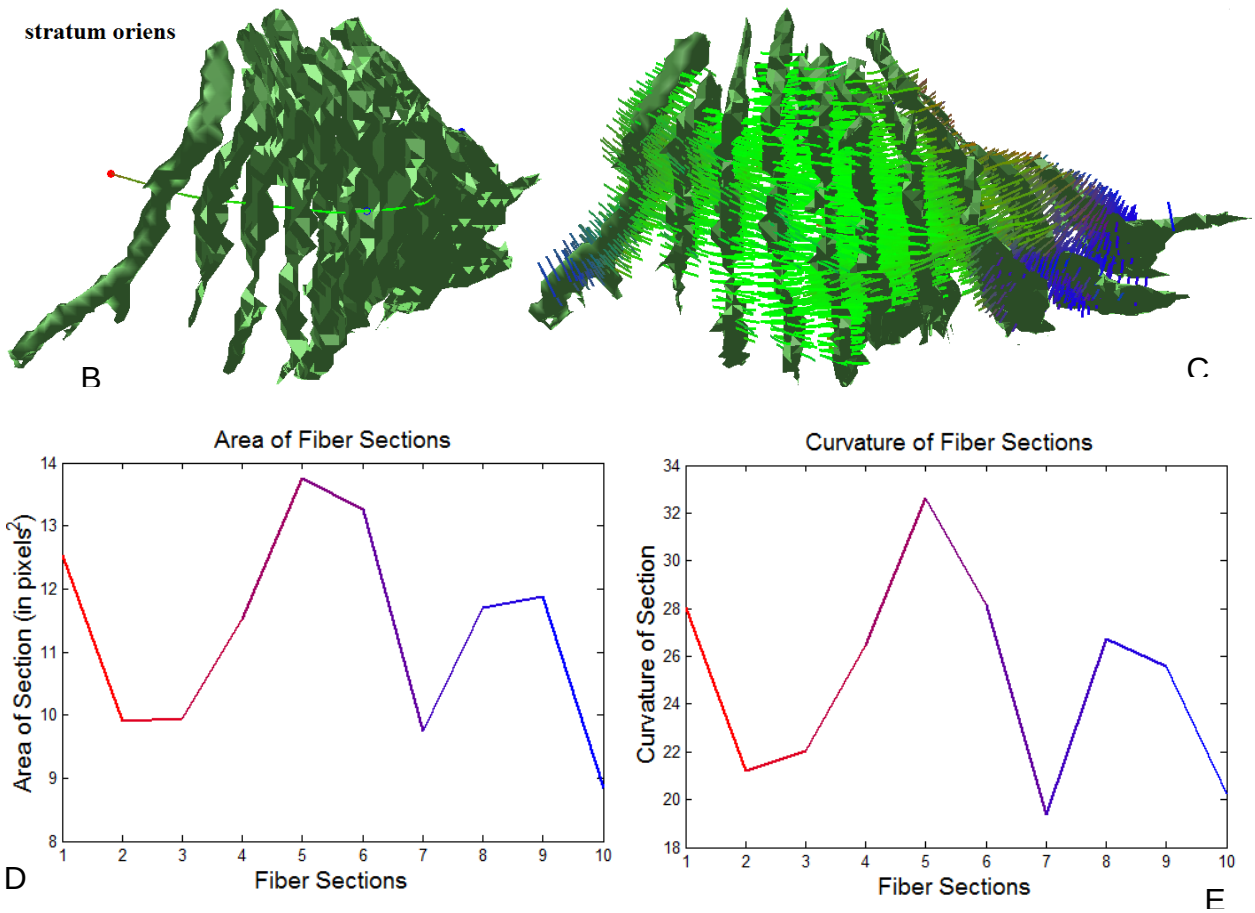

Figure 4-4. Results obtained from analysis of the rat hippocampus with seed point in the stratum oriens: [A] Shown is the colored FA map where the green, red and blue color indicate the direction of the underlying fibers being the horizontal, vertical or perpendicular (out of plane), respectively. The approximate location of the seed point within the stratum oriens is indicated by the yellow arrow. [B] The primary fiber was traced from the seed point (marked in red) and cost surfaces were at 10 different locations along the length of the primary fiber, from the seed point to the end point (blue). [C] The whole fiber bundle is depicted. [D] and [E] The change in the cross sectional area and curvature determined from the algorithm is plotted using red-blue color graded curve. The red-to-blue gradation indicates the distance along the fiber from the seed location to the end location.

4.4.3 Discussions

To help verify that the reconstructed bundle contained all possible fibers in the hippocampus region of interest, a zero eigenvector value was assigned to all the voxels

that had been covered while tracing the fiber bundle. The zero-valued eigenvectors appears as a black pixel (dot) in the colored FA plot.

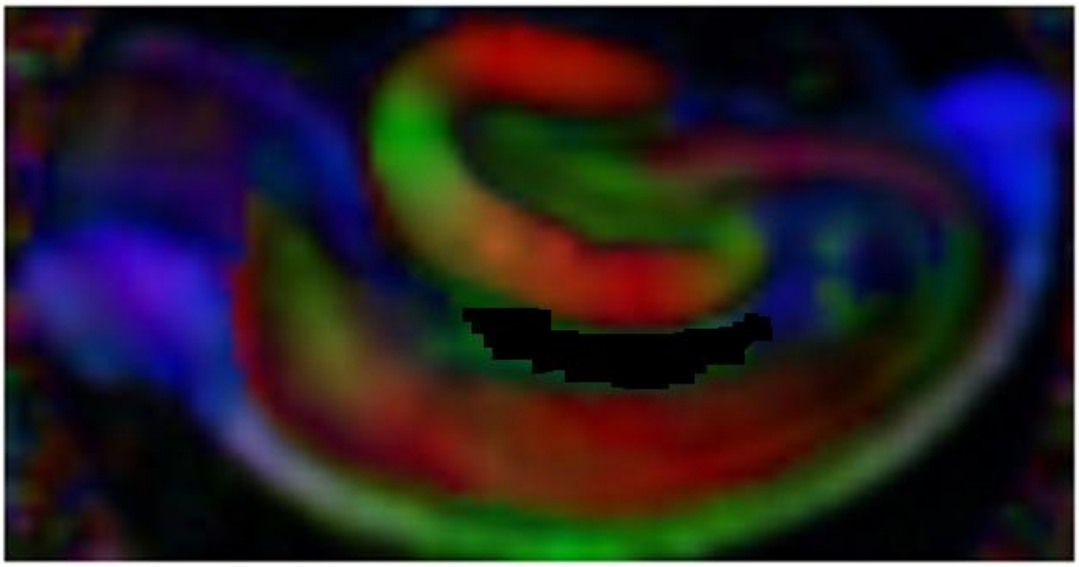

Figure 4-5. Visual depiction of the extent of the reconstructed fiber bundle in the stratum lacunosum-moleculare: the colored FA map is depicted with eigenvector value [0 0 0] for all the voxels covered in the fiber bundle. The region in black depicts approximately the bundle traced by the perpendicular fiber tracking method.

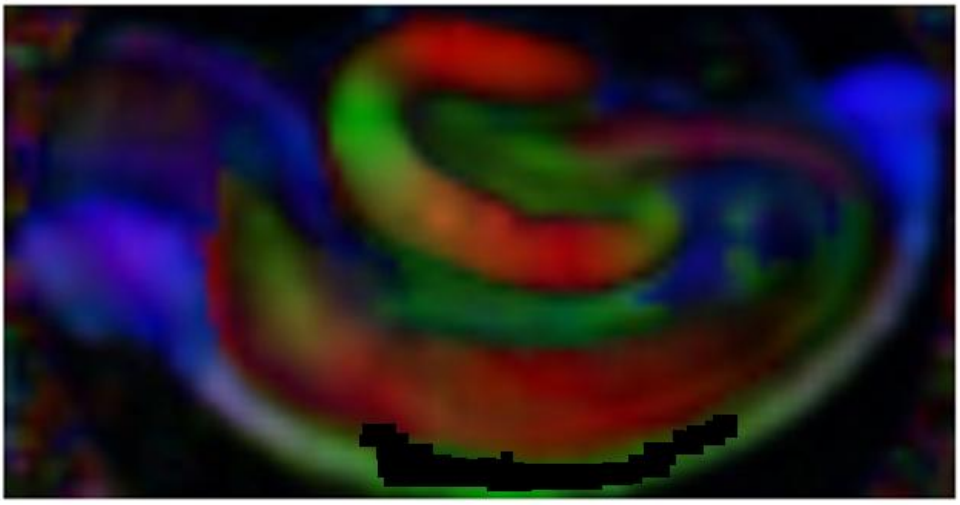

Figure 4-6. Visual depiction of the extent of the reconstructed fiber bundle in the Stratum oriens: the colored FA map is depicted with eigenvector value [0 0 0] for all the voxels covered in fiber bundle. The region in black depicts approximately the bundle traced by the perpendicular fiber tracking method.

From the above observation (Figure 4-5 and Figure 4-6) the calculated area and curvature used to construct the fiber bundle approximately fits the two regions, stratum lacunosum-moleculare and stratum oriens, of the rat hippocampus.

4.5 Control and Disease (Epilepsy) Rat Brain

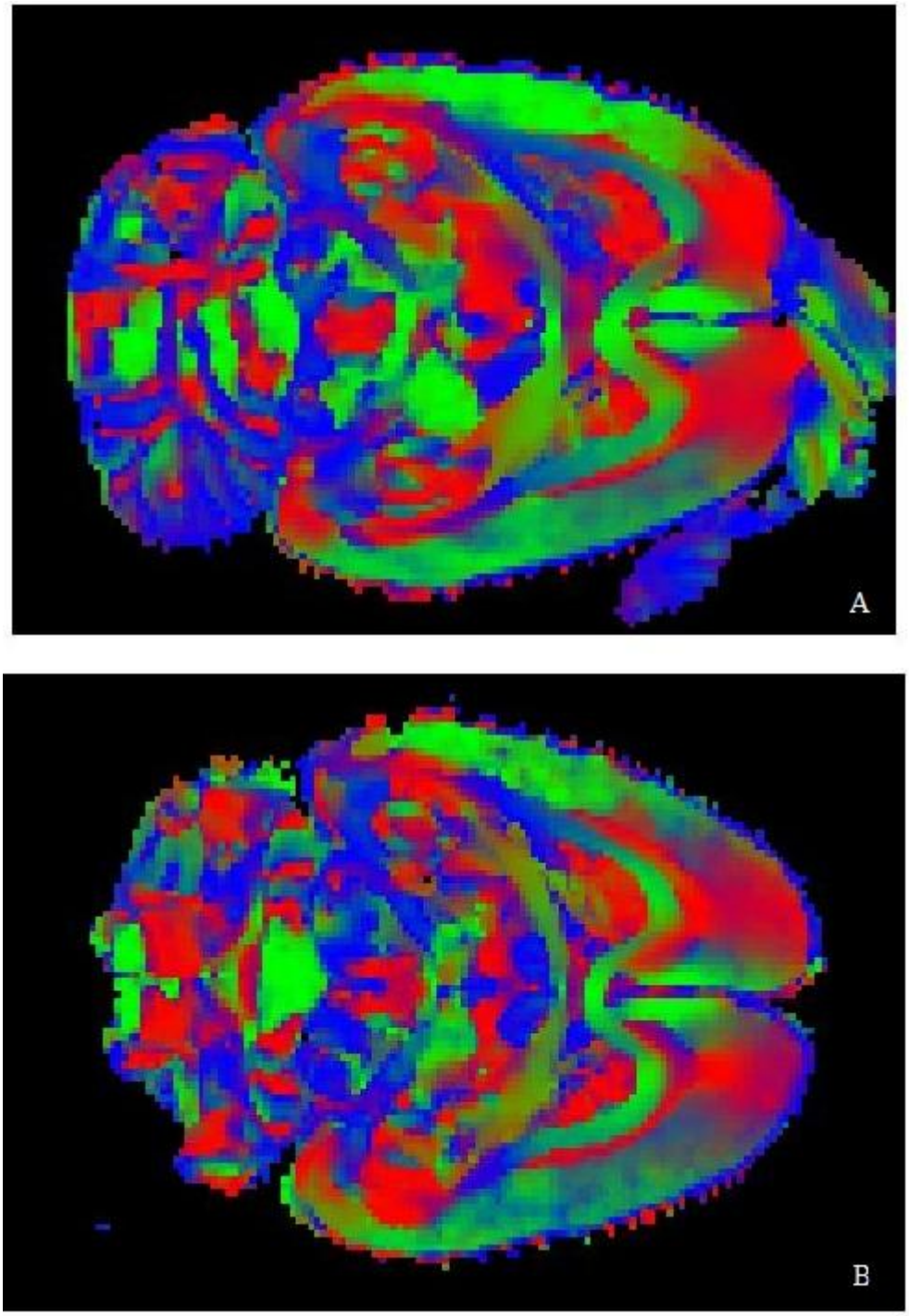

Figure 4-7. [A] Shown is the colored FA map of control rat brain dataset and [B] colored FA map of disease (epilepsy) rat brain where the green, red and blue color indicate the direction of the underlying fibers being the horizontal, vertical or perpendicular respectively.

4.5.1 Data Acquisition

The acquisition protocol [20] included 63 images collected with TR = 1500 ms, TE = 30 ms, 1 average, Δ = 17.65 ms, δ = 4.8 ms, spectral width = 55 KHz. Twelve contiguous slices of 0.9 mm thickness were imaged with a FOV of 30 mm × 30 mm and imaging matrix size of 100 × 100. Low-diffusion-weighted image data sets (b value of 100 s/mm^2) were acquired in 6 directions and high-diffusion-weighted image data sets (b value of 800 s/mm^2) were acquired in 21 directions, determined from the level 1 triangular subdivision of an icosahedron tessellated onto the surface of a unit hemisphere.

4.5.2 Fiber Bundle Analysis of Control and Disease Rat Brain

The algorithm was performed at 12 different points on the two rat brain datasets. In each run, a seed point (manually selected) was placed on a healthy rat brain (37th slice) and epilepsy rat brain (38th slice) and a primary fiber was traced from seed point using deterministic tractography, and 4 cost surfaces were constructed along the length of the primary fiber (not shown). The average of all 4 cost surface cross sectional areas were taken at 5 different cost thresholds (0.4, 0.5, 0.6, 0.7, 0.8). All of the fibers passing along the cost surfaces were traced to ensure that the surfaces did not include the fibers outside the bundle region (not shown). The output, plots of area at each threshold, for control as well as disease brain were obtained from the algorithm and are demonstrated in the following figures.

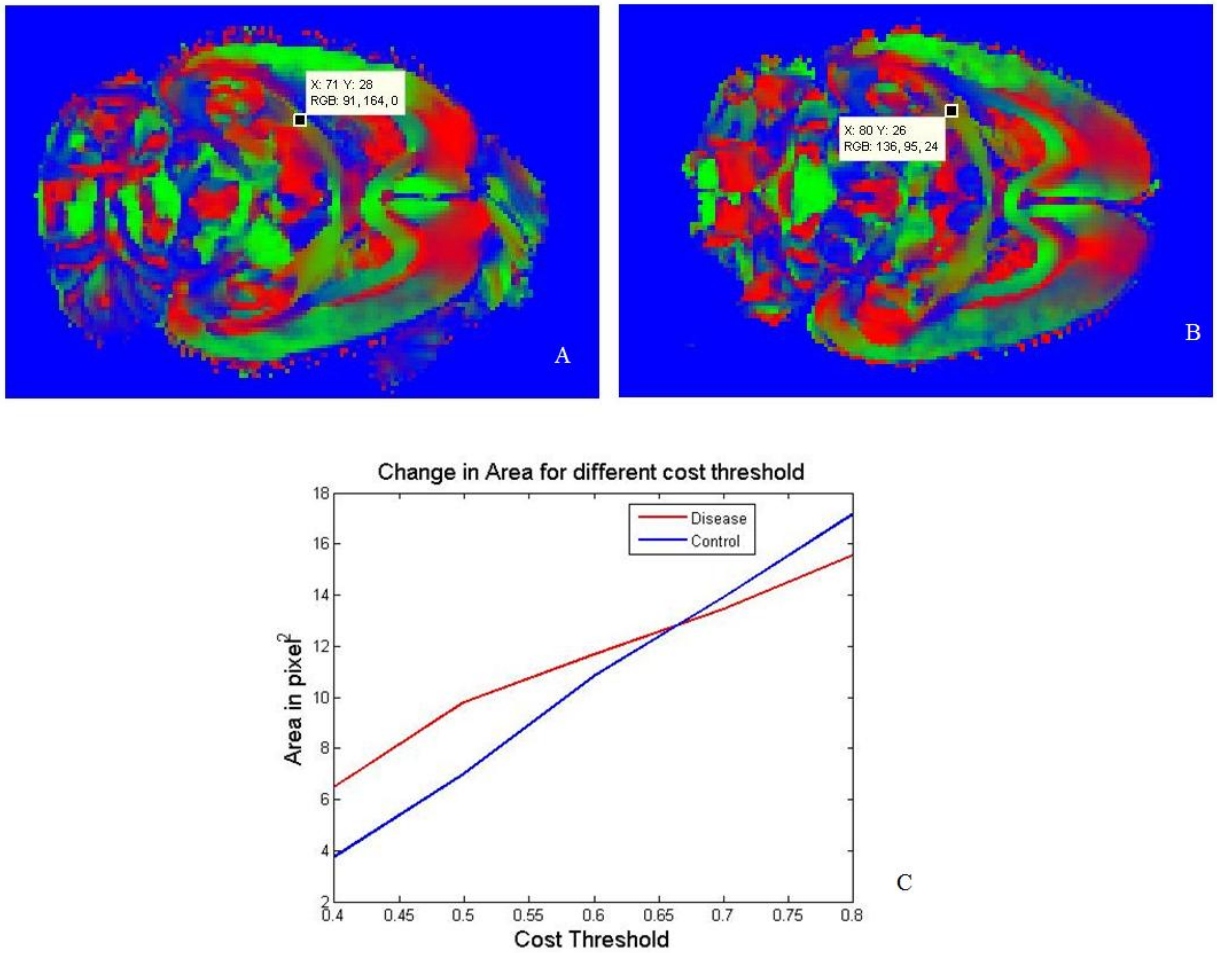

Figure 4-8. Results obtained from analysis of the rat brain with seed point shown with black marker: [A] and [B] Shown is the colored FA map of control and epileptic rat brain, respectively, where the green, red and blue color indicates the direction of the underlying fibers being the horizontal, vertical or perpendicular respectively. [C] The change in the cross sectional area for 5 different cost threshold in a healthy brain (blue color) and epilepsy (red color) determined from the algorithm is plotted.

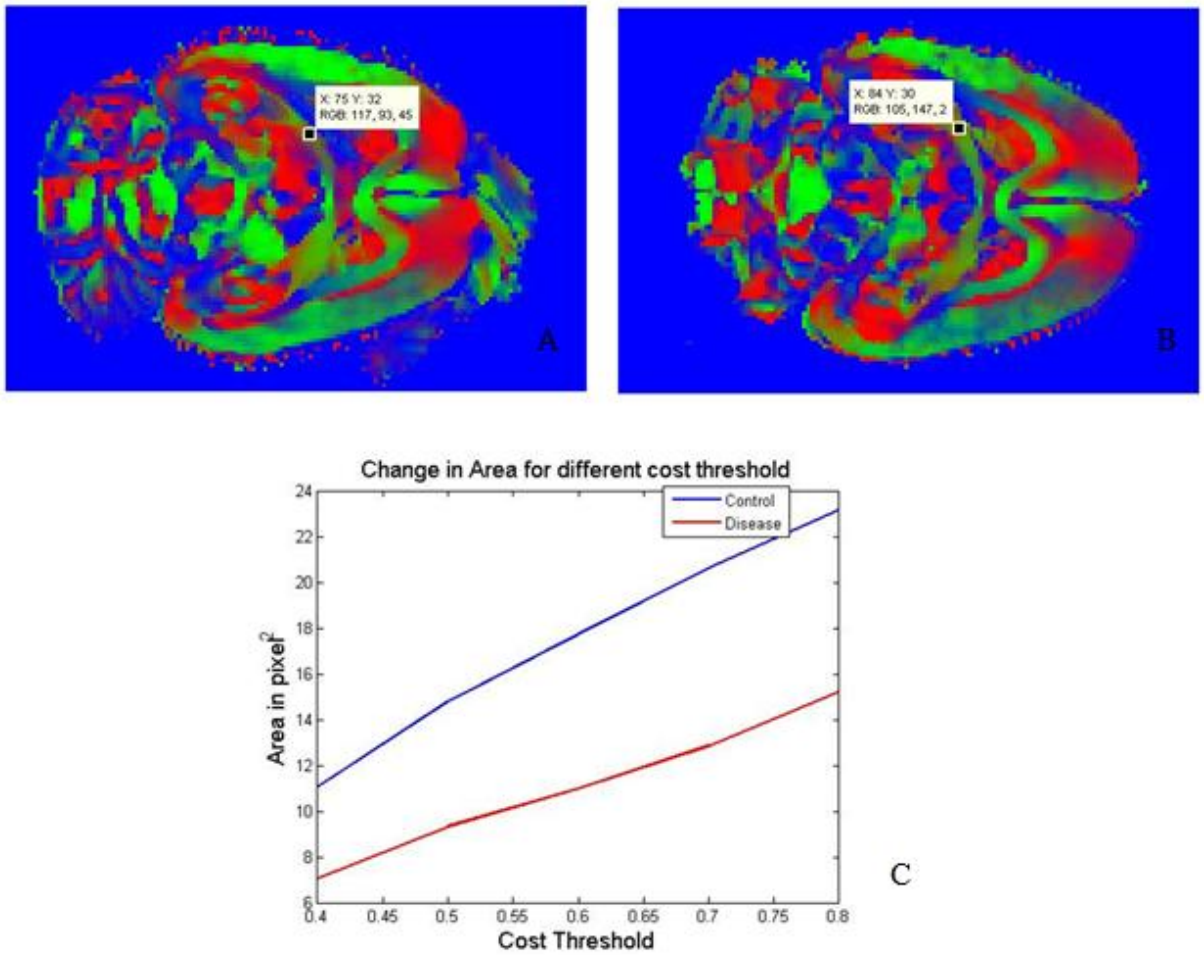

Figure 4-9. Results obtained from analysis of the rat brain with seed point shown with black marker: [A] and [B] Shown is the colored FA map of control and epileptic rat brain, respectively, where the green, red and blue color indicates the direction of the underlying fibers being the horizontal, vertical or perpendicular respectively. [C] The change in the cross sectional area for 5 different cost threshold in a healthy brain (blue color) and epilepsy (red color) determined from the algorithm is plotted.

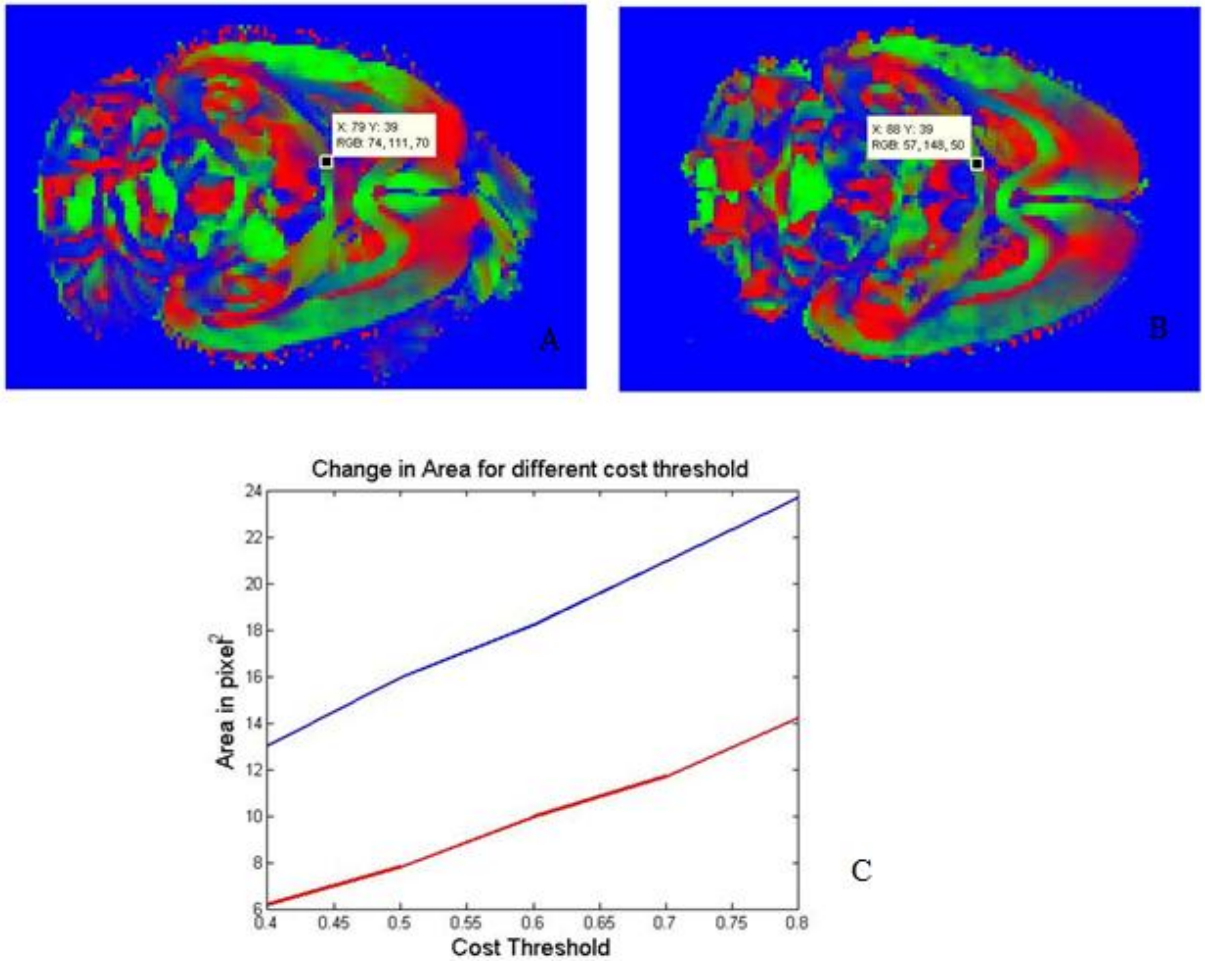

Figure 4-10. Results obtained from analysis of the rat brain with seed point shown with black marker: [A] and [B] Shown is the colored FA map of control and epileptic rat brain, respectively, where the green, red and blue color indicates the direction of the underlying fibers being the horizontal, vertical or perpendicular respectively. [C] The change in the cross sectional area for 5 different cost threshold in a healthy brain (blue color) and epilepsy (red color) determined from the algorithm is plotted.

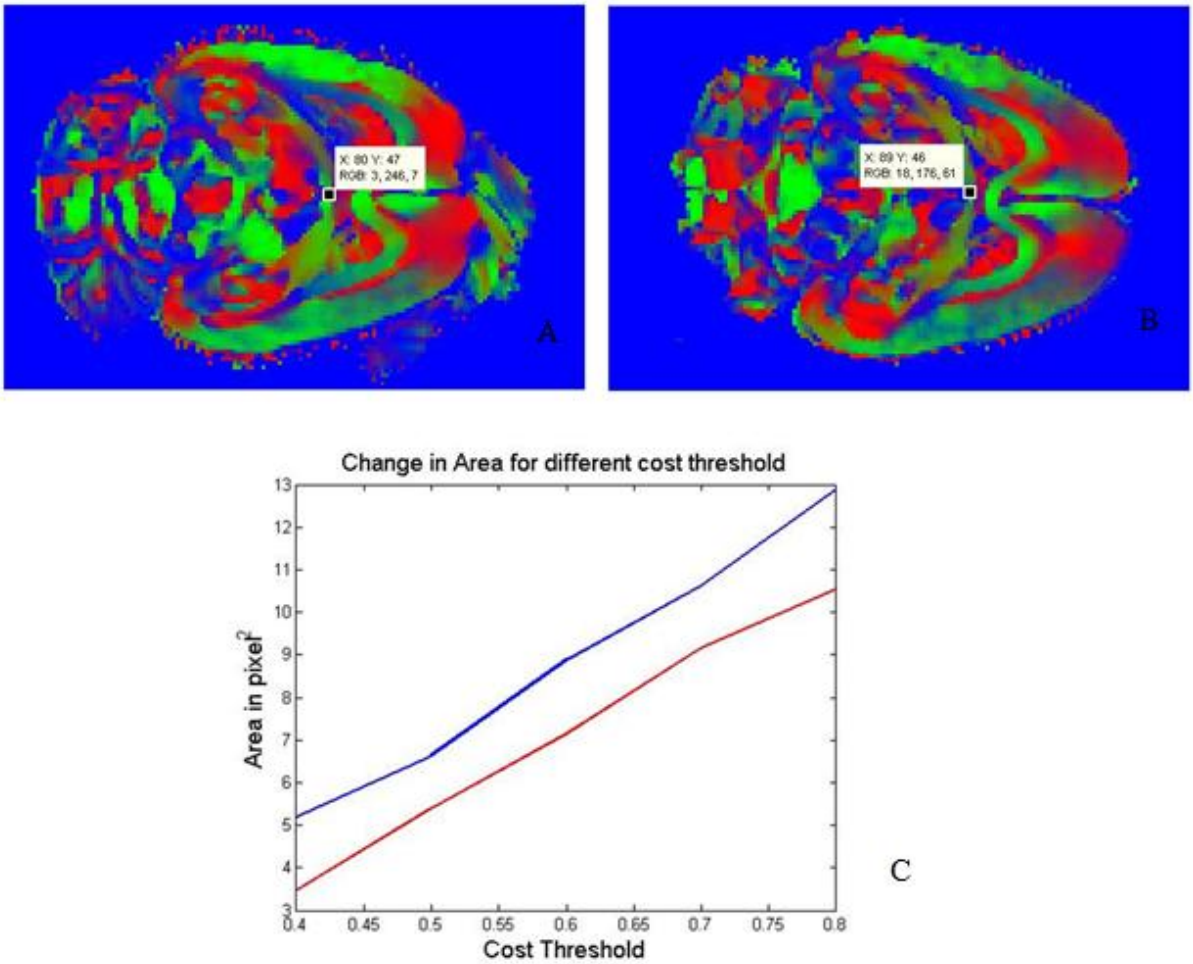

Figure 4-11. Results obtained from analysis of the rat brain with seed point shown with black marker: [A] and [B] Shown is the colored FA map of control and epileptic rat brain, respectively, where the green, red and blue color indicates the direction of the underlying fibers being the horizontal, vertical or perpendicular respectively. [C] The change in the cross sectional area for 5 different cost threshold in a healthy brain (blue color) and epilepsy (red color) determined from the algorithm is plotted.

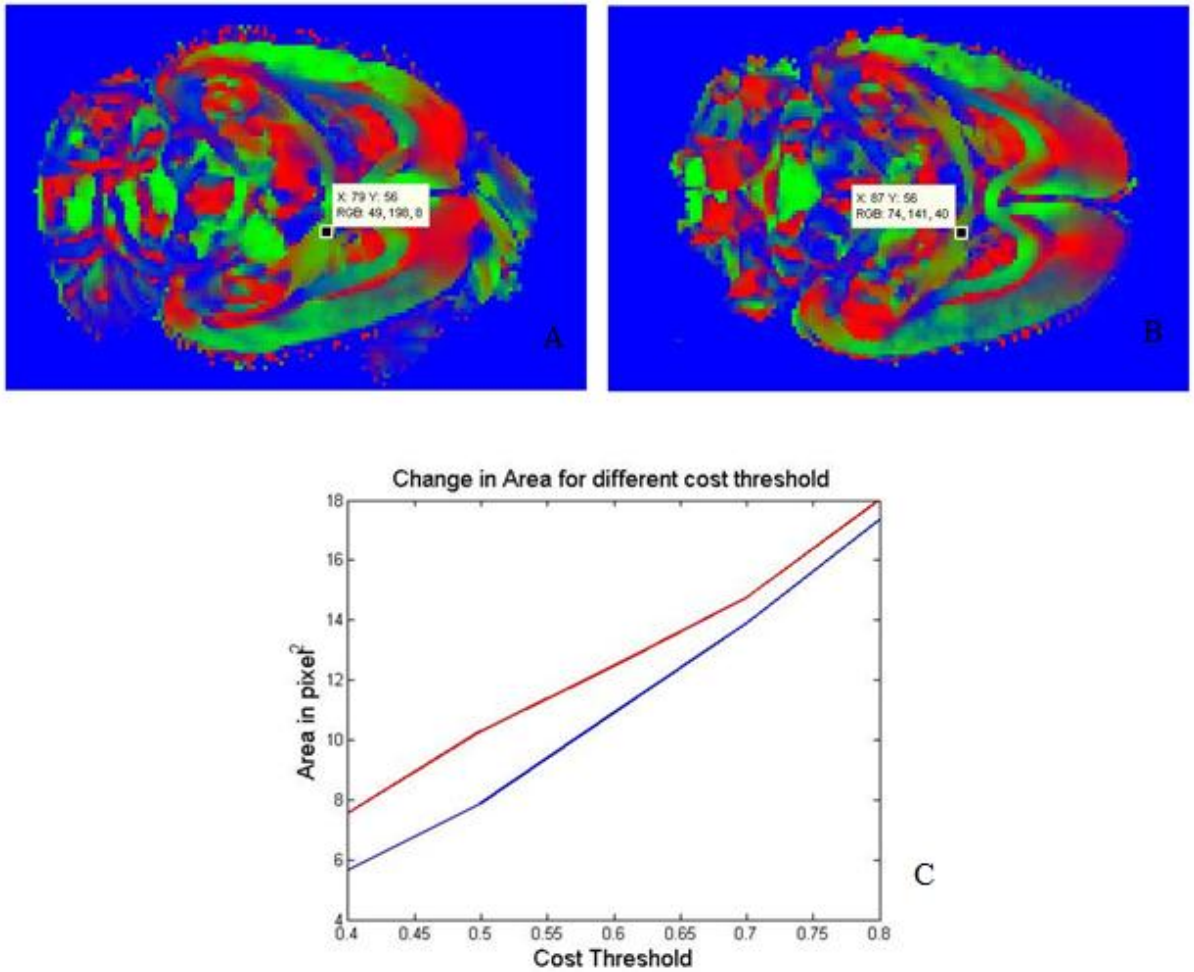

Figure 4-12. Results obtained from analysis of the rat brain with seed point shown with black marker: [A] and [B] Shown is the colored FA map of control and epileptic rat brain, respectively, where the green, red and blue color indicates the direction of the underlying fibers being the horizontal, vertical or perpendicular respectively. [C] The change in the cross sectional area for 5 different cost threshold in a healthy brain (blue color) and epilepsy (red color) determined from the algorithm is plotted.

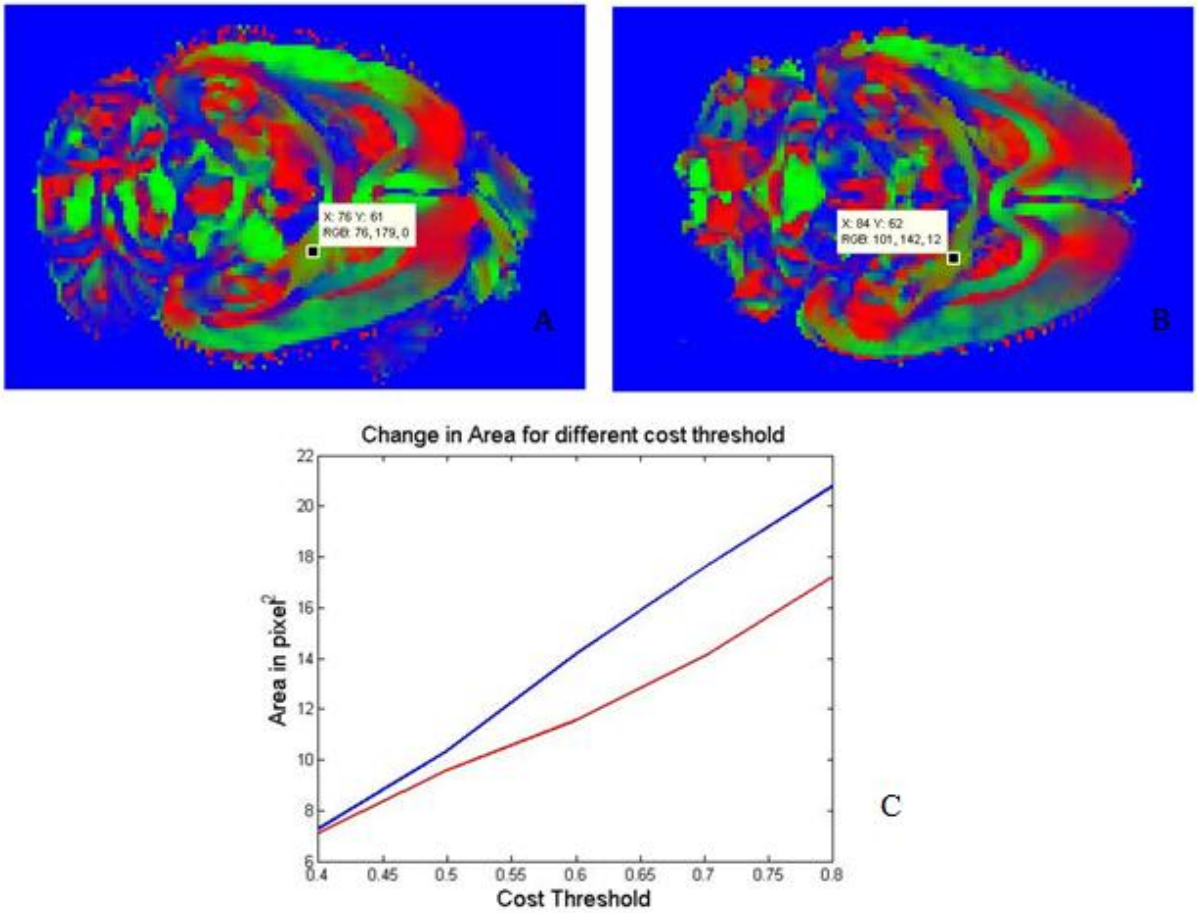

Figure 4-13. Results obtained from analysis of the rat brain with seed point shown with black marker: [A] and [B] Shown is the colored FA map of control and epileptic rat brain, respectively, where the green, red and blue color indicates the direction of the underlying fibers being the horizontal, vertical or perpendicular respectively. [C] The change in the cross sectional area for 5 different cost threshold in a healthy brain (blue color) and epilepsy (red color) determined from the algorithm is plotted.

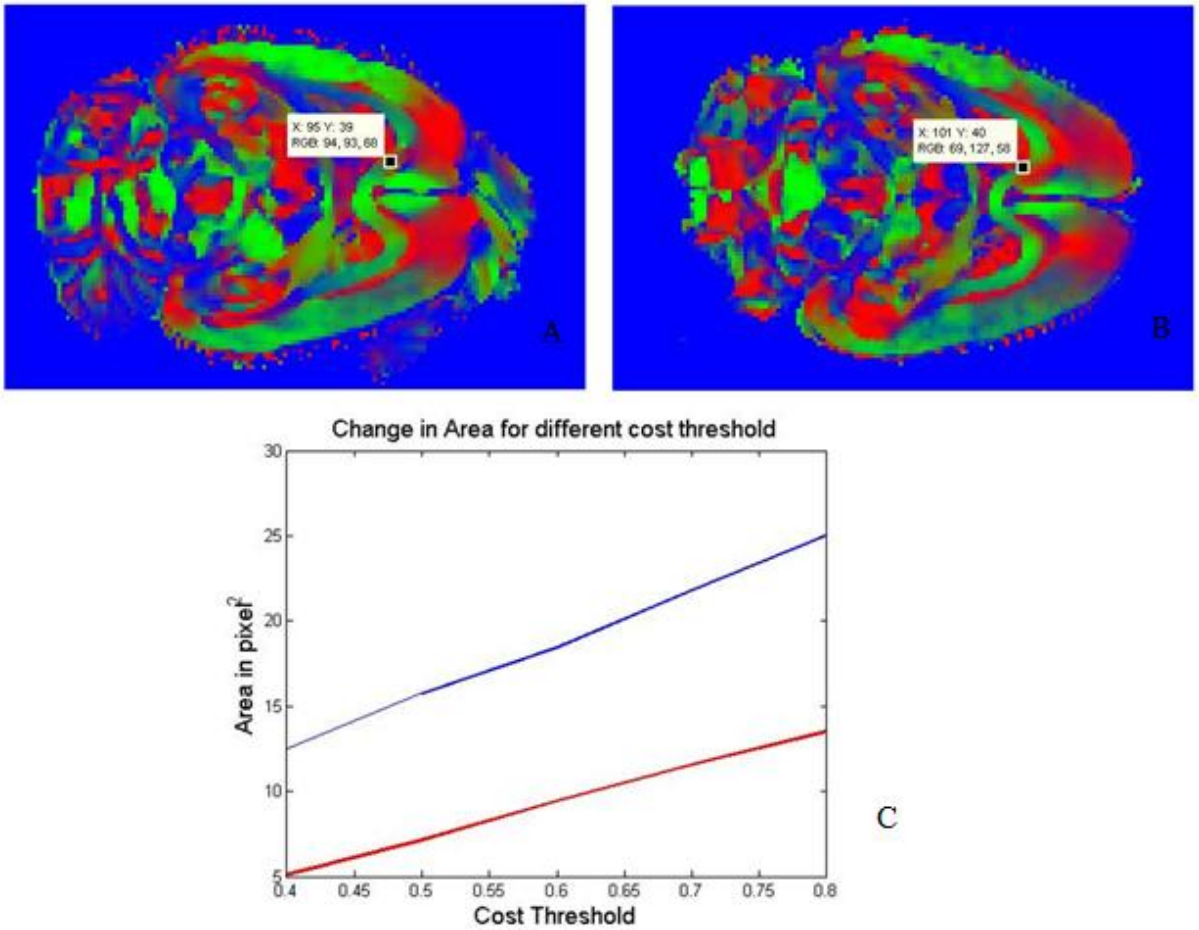

Figure 4-14. Results obtained from analysis of the rat brain with seed point shown with black marker: [A] and [B] Shown is the colored FA map of control and epileptic rat brain, respectively, where the green, red and blue color indicates the direction of the underlying fibers being the horizontal, vertical or perpendicular respectively. [C] The change in the cross sectional area for 5 different cost threshold in a healthy brain (blue color) and epilepsy (red color) determined from the algorithm is plotted.

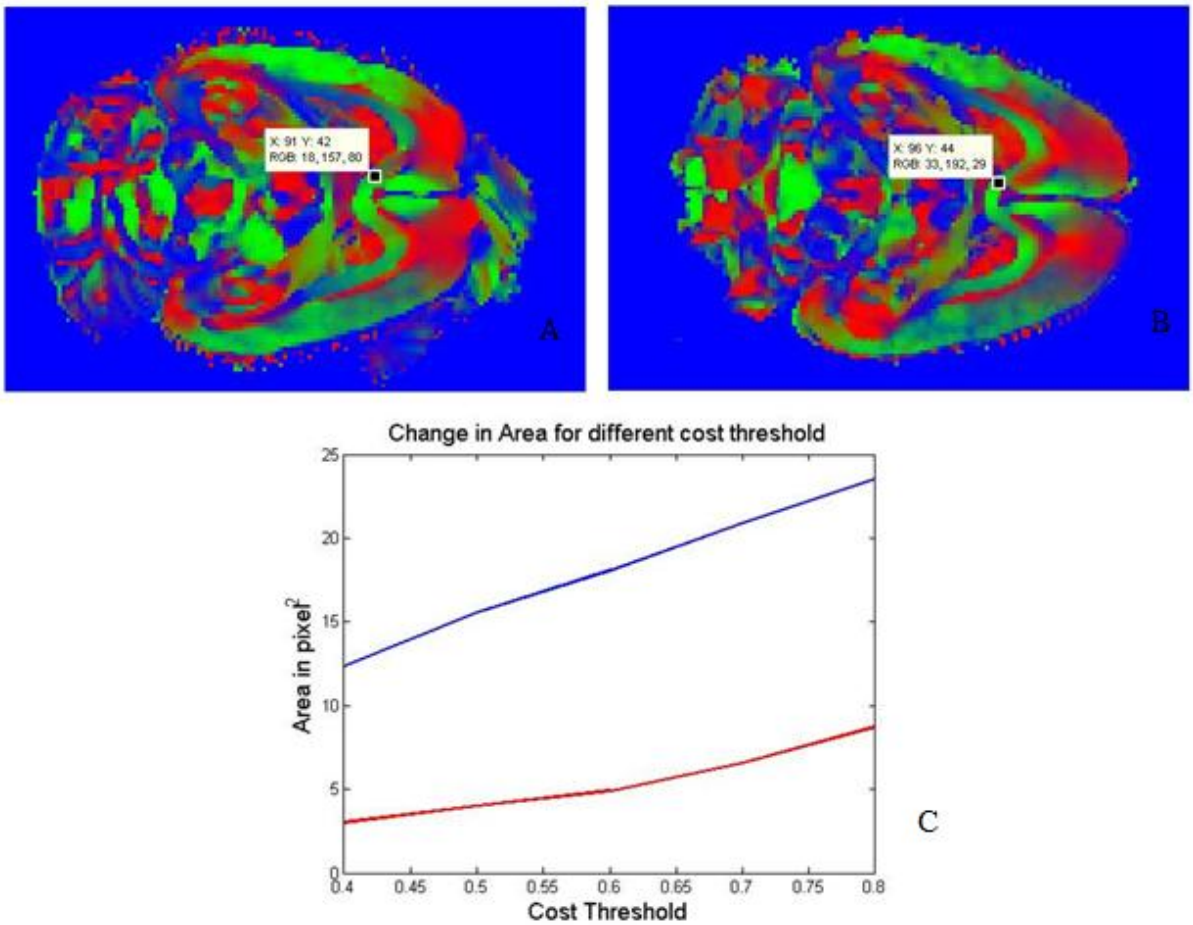

Figure 4-15. Results obtained from analysis of the rat brain with seed point shown with black marker: [A] and [B] Shown is the colored FA map of control and epileptic rat brain, respectively, where the green, red and blue color indicates the direction of the underlying fibers being the horizontal, vertical or perpendicular respectively. [C] The change in the cross sectional area for 5 different cost threshold in a healthy brain (blue color) and epilepsy (red color) determined from the algorithm is plotted.

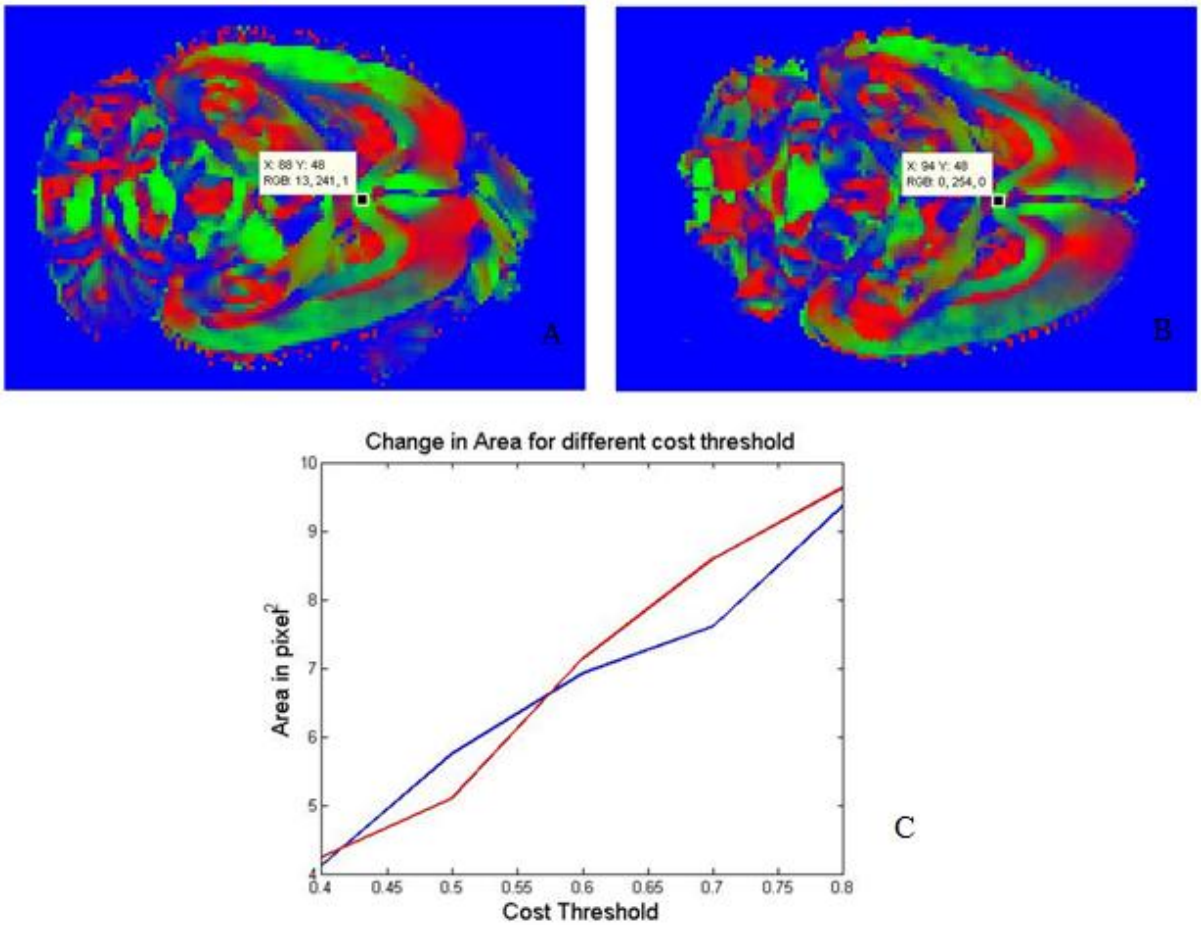

Figure 4-16. Results obtained from analysis of the rat brain with seed point shown with black marker: [A] and [B] Shown is the colored FA map of control and epileptic rat brain, respectively, where the green, red and blue color indicates the direction of the underlying fibers being the horizontal, vertical or perpendicular respectively. [C] The change in the cross sectional area for 5 different cost threshold in a healthy brain (blue color) and epilepsy (red color) determined from the algorithm is plotted.

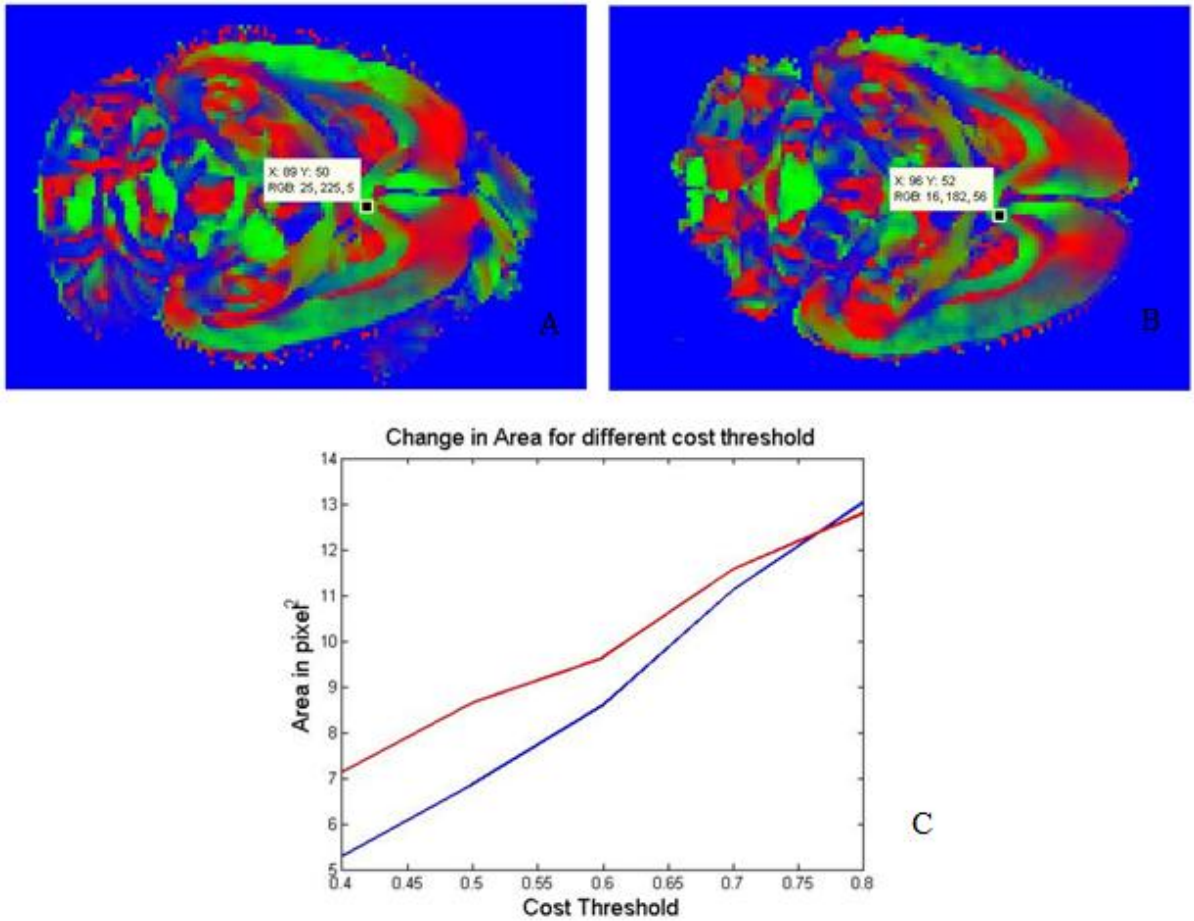

Figure 4-17. Results obtained from analysis of the rat brain with seed point shown with black marker: [A] and [B] Shown is the colored FA map of control and epileptic rat brain, respectively, where the green, red and blue color indicates the direction of the underlying fibers being the horizontal, vertical or perpendicular respectively. [C] The change in the cross sectional area for 5 different cost threshold in a healthy brain (blue color) and epilepsy (red color) determined from the algorithm is plotted.

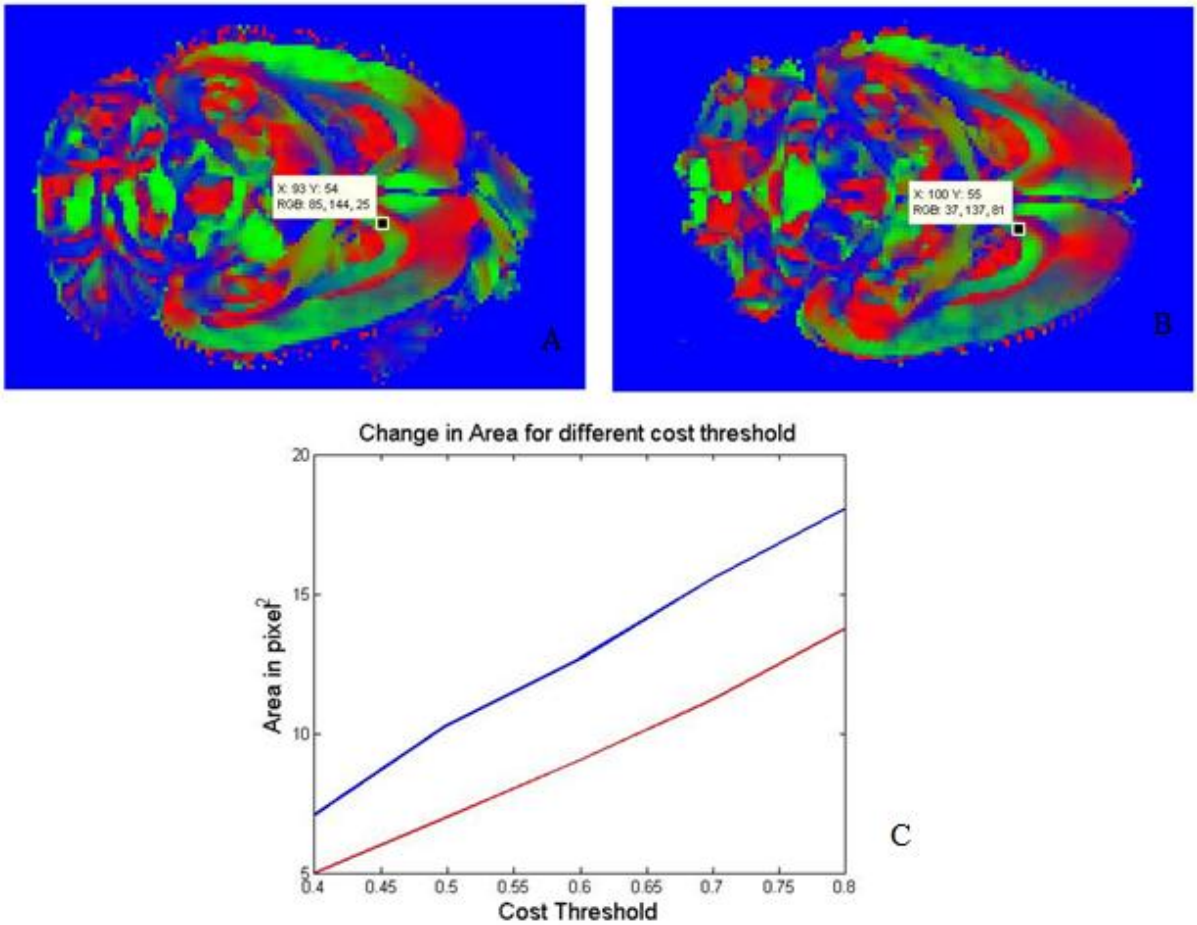

Figure 4-18. Results obtained from analysis of the rat brain with seed point shown with black marker: [A] and [B] Shown is the colored FA map of control and epileptic rat brain, respectively, where the green, red and blue color indicates the direction of the underlying fibers being the horizontal, vertical or perpendicular respectively. [C] The change in the cross sectional area for 5 different cost threshold in a healthy brain (blue color) and epilepsy (red color) determined from the algorithm is plotted.

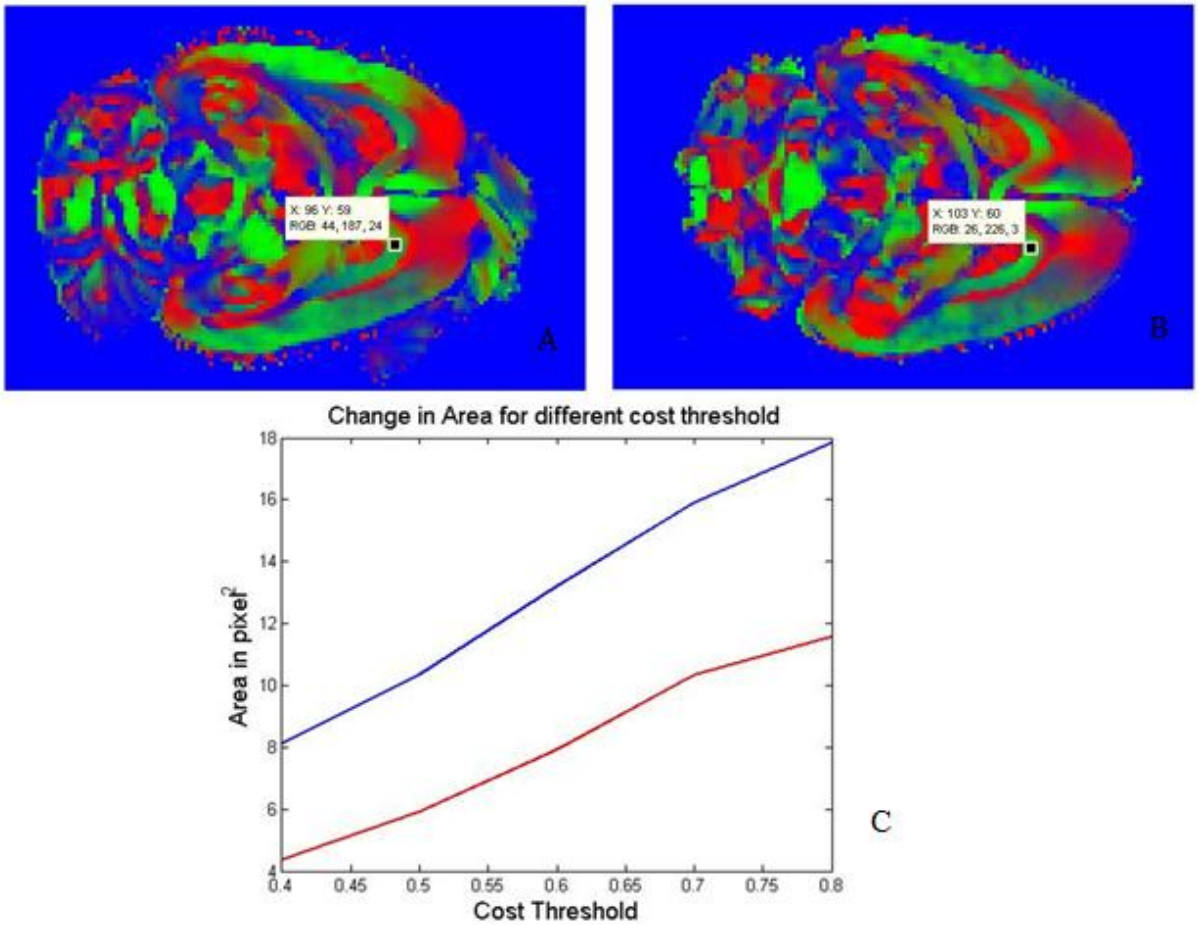

Figure 4-19. Results obtained from analysis of the rat brain with seed point shown with black marker: [A] and [B] Shown is the colored FA map of control and epileptic rat brain, respectively, where the green, red and blue color indicates the direction of the underlying fibers being the horizontal, vertical or perpendicular respectively. [C] The change in the cross sectional area for 5 different cost threshold in a healthy brain (blue color) and epilepsy (red color) determined from the algorithm is plotted.

4.5.3 Discussion

After running algorithm at all of the above mentioned points, we observe difference in the fiber bundle area between healthy and epileptic rats in the marked (circled white) regions, shown in Figure 4-20.

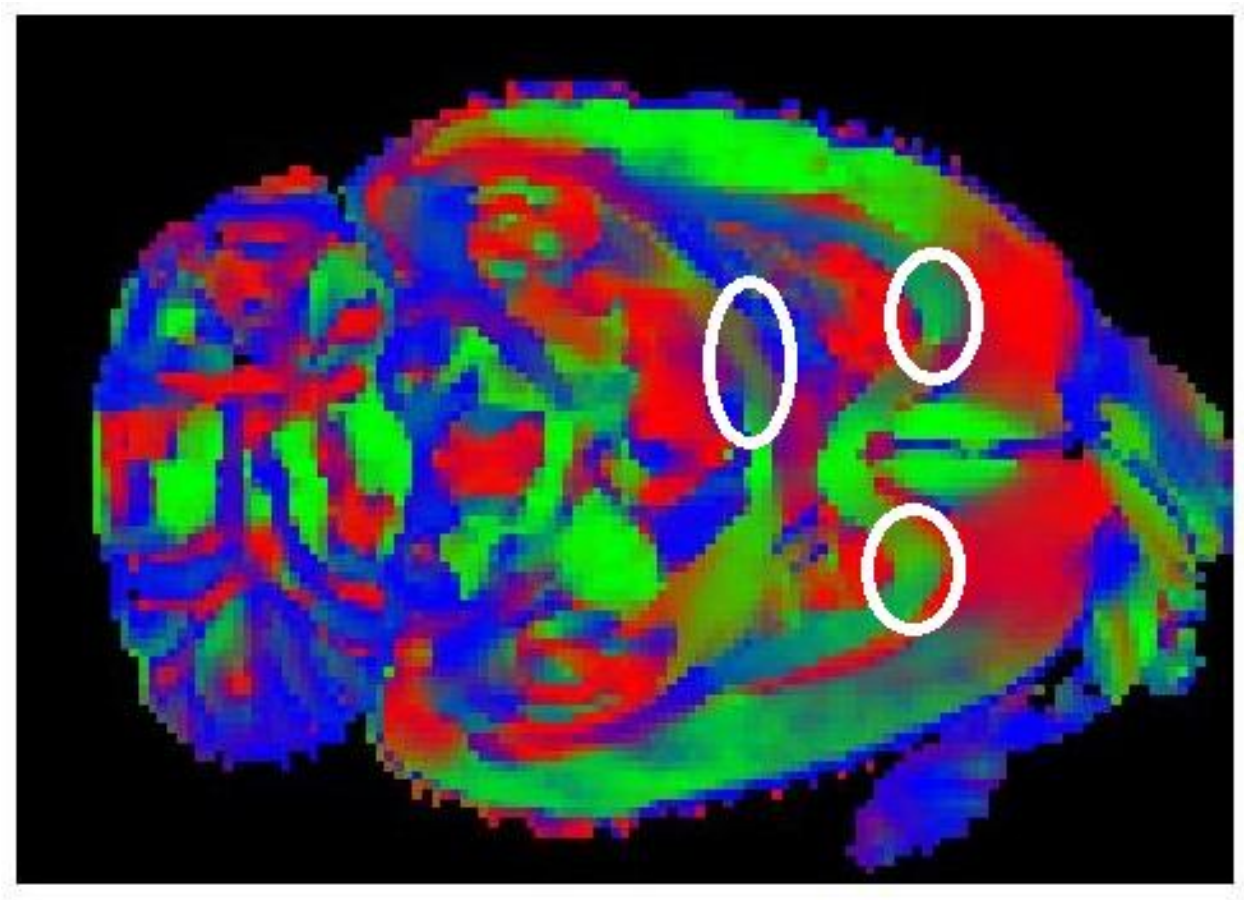

Figure 4-20. Depicts the colored FA diagram of healthy rat brain where the green, red and blue color indicates the direction of fiber in horizontal, vertical or perpendicular respectively. The white ellipses indicate regions where differences in the fiber bundle area between healthy and epileptic rats were observed.

CHAPTER 5
CONCLUSIONS AND FUTURE WORK

5.1 Conclusions

In conclusion, the results of my experiments obtained from real DTI datasets of rat hippocampus, diseased (epilepsy) and control (healthy) brain demonstrate the use of method. Furthermore, verification of the algorithm on synthetic datasets, including linearly increasing fibers along a fiber bundle, branching fibers and crossing fibers, demonstrate the accuracy of our technique.

The algorithm produces interactively comprehensive statistics on area and curvature along fiber bundles with potential for near real time clinical use. The algorithm is successful in tracking fibers in directions other than theprincipal direction of diffusion and provides new information on local patterns of diffusion. The technique can be used as a tool for fiber bundle segmentation, for neural fiber analysis, and potentially as a biomarker for various brain disease that involve some kind of change in white matter, including Alzheimer's Disease, Parkinson's Disease, epilepsy, autism and other dementias.

5.2 Limitations

A major limitation of this work was the algorithm's dependency on MR-DTI data and the many limitations associated with MR-DTI. First, MR-DTI is incapable of differentiating efferent nerves, anterograde and retrograde pathways, inhibitory and excitatory connections as well as direct-indirect routes in data. Second, the regions of fiber crossing, smaller pathways and fibers interrupted by synapses may not be detected with DTI. Last, long and complex nerve fiber pathways are less likely to be traced.

Another potential problem is the need to optimize the cost threshold for different cases. For example, the image quality and resolution of MR data sets can differ depending upon the scanner's magnetic field strength, the scanning time available and the number of receive coils, and a different optimal threshold may be needed for each case.Although in most practical cases the error due to small deviation from the optimal threshold is not dramatic, a different cost threshold was used for each of the animal and synthetic data sets is presented here.

Thus, future work should be directed towards overcoming the above limitations to derive more accurate and reproducible results and interpretations.

5.3 Future Work

5.3.1 Improvement of Perpendicular Fiber Tracking Method

The errors evident in the analysis of the synthetic crossing fiber data set may be overcome with improved MR-DTI acquisition and reconstruction. High-angular-resolution diffusion imaging (HARDI) has been demonstrated to permit the identification of multiple crossing fibers within the same voxel. Perpendicular fiber tracking based on HARDI is expected to allow us to compute the fiber metrics for regions of fiber crossing. HARDI data may also enable improved the analysis of small pathways and long tortuous pathways.

Future work should be directed towards implementing a global cost threshold that can be run effectively on various data sets. One possible approach would be to employ self-learning (machine learning) feature in the algorithm.

5.3.2 Application on Real Datasets

Since the algorithm was successfully validated on different synthetic data sets and was also applied to real brain data sets, the method can be applied to some diseased

brains (Alzheimer's Disease, epilepsy, Parkinson's Disease, cancer) data sets to diagnose changes in the fiber geometry.

LIST OF REFERENCES

[1] J. S. Duncan, “Imaging the Brain’s Highways—Diffusion Tensor Imaging in Epilepsy,” *Epilepsy Curr*, vol. 8, no. 4, pp. 85–89, Jul. 2008.

[2] M. S. Buchsbaum, J. Friedman, B. R. Buchsbaum, K.-W. Chu, E. A. Hazlett, R. Newmark, J. S. Schneiderman, Y. Torosjan, C. Tang, P. R. Hof, D. Stewart, K. L. Davis, and J. Gorman, “Diffusion tensor imaging in schizophrenia,” *Biol. Psychiatry*, vol. 60, no. 11, pp. 1181–1187, Dec. 2006.

[3] D. A. Medina and M. Gaviria, “Diffusion tensor imaging investigations in Alzheimer’s disease: the resurgence of white matter compromise in the cortical dysfunction of the aging brain,” *Neuropsychiatr Dis Treat*, vol. 4, no. 4, pp. 737–742, Aug. 2008.

[4] L.-L. Chan, H. Rumpel, K. Yap, E. Lee, H.-V. Loo, G.-L. Ho, S. Fook-Chong, Y. Yuen, and E.-K. Tan, “Case control study of diffusion tensor imaging in Parkinson’s disease,” *J. Neurol. Neurosurg. Psychiatr.*, vol. 78, no. 12, pp. 1383–1386, Dec. 2007.

[5] R. A. . Krishnan, D. Davis, P. Okunieff, and W. O’Dell, “Random walk model based on DTI for predicting the microscopic spread of gliomas,” in *5th IEEE International Symposium on Biomedical Imaging: From Nano to Macro, 2008. ISBI 2008*, 2008, pp. 891–894.

[6] “Disease Statistics,” *Oregon Health & Science University*. [Online]. Available: http://www.ohsu.edu/xd/education/schools/research-institutes/brain-institute/brain-awareness/about/disease-statistics.cfm. [Accessed: 01-Mar-2012].

[7] “Latest Facts & Figures Report | Alzheimer’s Association.” [Online]. Available: http://www.alz.org/alzheimers_disease_facts_and_figures.asp. [Accessed: 18-Feb-2012].

[8] “Brain Cancer.” [Online]. Available: http://www.nlm.nih.gov/medlineplus/braincancer.html#cat22. [Accessed: 01-Mar-2012].

[9] D. N. Louis, H. Ohgaki, O. D. Wiestler, W. K. Cavenee, P. C. Burger, A. Jouvet, B. W. Scheithauer, and P. Kleihues, “The 2007 WHO Classification of Tumours of the Central Nervous System,” *Acta Neuropathol*, vol. 114, no. 2, pp. 97–109, Aug. 2007.

[10] P. J. Basser, J. Mattiello, and D. LeBihan, “MR diffusion tensor spectroscopy and imaging,” *Biophysical Journal*, vol. 66, no. 1, pp. 259–267, Jan. 1994.

[11] P. J. Basser, S. Pajevic, C. Pierpaoli, J. Duda, and A. Aldroubi, “In vivo fiber tractography using DT- MRI data,” *Magnetic Resonance in Medicine*, vol. 44, no. 4, pp. 625–632, Oct. 2000.

[12] S. Mori, B. J. Crain, V. P. Chacko, and P. C. M. Van Zijl, “Three- dimensional tracking of axonal projections in the brain by magnetic resonance imaging,” *Annals of Neurology*, vol. 45, no. 2, pp. 265–269, Feb. 1999.

[13] A. A. Qazi, A. Radmanesh, L. O’Donnell, G. Kindlmann, S. Peled, S. Whalen, C.-F. Westin, and A. J. Golby, “Resolving crossings in the corticospinal tract by two-tensor streamline tractography,” *Neuroimage*, vol. 47, no. Suppl 2, pp. T98–106, Aug. 2009.

[14] U. Bozkaya and B. Acar, “SMT: Split and Merge Tractography for DT-MRI,” in *Medical Image Computing and Computer-Assisted Intervention – MICCAI 2007*, vol. 4792, N. Ayache, S. Ourselin, and A. Maeder, Eds. Berlin, Heidelberg: Springer Berlin Heidelberg, pp. 153–160.

[15] M. Reisert, I. Mader, C. Anastasopoulos, M. Weigel, S. Schnell, and V. Kiselev, “Global fiber reconstruction becomes practical,” *Neuroimage*, vol. 54, no. 2, pp. 955–962, Jan. 2011.

[16] B. W. Kreher, I. Mader, and V. G. Kiselev, “Gibbs tracking: a novel approach for the reconstruction of neuronal pathways,” *Magn Reson Med*, vol. 60, no. 4, pp. 953–963, Oct. 2008.

[17] P. Fillard, C. Poupon, and J.-F. Mangin, “A novel global tractography algorithm based on an adaptive spin glass model.,” *Medical Image Computing and Computer-Assisted Intervention*, vol. 12, no. Pt 1, pp. 927–934, 2009.

[18] E. N. Mortensen and W. A. Barrett, “Interactive Segmentation with Intelligent Scissors,” *Graphical Models and Image Processing*, vol. 60, no. 5, pp. 349–384, Sep. 1998.

[19] A. Barmpoutis, B. C. Vemuri, T. M. Shepherd, and J. R. Forder, “Tensor Splines for Interpolation and Approximation of DT-MRI With Applications to Segmentation of Isolated Rat Hippocampi,” *IEEE Transactions on Medical Imaging*, vol. 26, no. 11, pp. 1537–1546, Nov. 2007.

[20] M. B. Parekh, P. R. Carney, H. Sepulveda, W. Norman, M. King, and T. H. Mareci, “Early MR diffusion and relaxation changes in the parahippocampal gyrus precede the onset of spontaneous seizures in an animal model of chronic limbic epilepsy,” *Experimental Neurology*, vol. 224, no. 1, pp. 258–270, Jul. 2010.

BIOGRAPHICAL SKETCH

Siddharth Ray received his Bachelor of Engineering in Biomedical from Shri Govindram Sekseriya Institute of Technology and Science (SGSITS) in 2006. He began graduate studies at the University of Florida in 2011. He pursued his research in the area of understanding the nerve fiber bundle using Magnetic Resonance Diffusion Tensor Imaging under guidance of Dr. Walter G. O'Dell and Dr. Angelos Barmpoutis since March 2011.